Electronic and optical properties of pristine and Nb doped TiO_2: A DFT study

Roll: 161303
Session : 2016-2017

Report submitted to the Department of Physics at
Jashore University of Science and Technology
in partial fulfillment of the requirements
for the degree of Bachelor of Science
with Honours in Physics

Abstract

TiO_2 has been widely studied because of its fascinating general properties in a wide range of fields with chemical changes, photo-catalysis, medication agent, environmental purification, and nano-fluid application which has a great effect on the standard of life. Because of its excellent optical properties, whiteness, and high refractive index, it has been widely used as sunscreen and white pigment for a long time. It is also used for detecting high-temperature ferromagnetic semiconductors. We follow the Full Potential Linear Augmented Plane Wave (FP-LAPW) method for our calculation based on Density Functional Theory (DFT). We use both PBE and mBJ potential for solving Kohn-Sham equation. In our current study, we tried to find out the electronic and optical properties of rutile and anatase TiO_2 and then we dope 25% Nb within rutile TiO_2. We tried to make a comparison between the changes in electronic and optical properties of rutile and $Ti_{0.75}Nb_{0.25}O_2$. TiO_2 is mainly a UV light absorber. When Nb is doped within pristine TiO_2, its absorptivity and conductivity increases in the visible region. TiO_2 shows non-metallic behavior when it is pure. For 25% dopant Nb, it turns into metal. It can be used to prepare highly efficient UV-absorbing thin-film coatings for the protection of organic materials against photodegradation.

Acknowledgements

Firstly, I praise and thank Almighty Allah, the Lord of the worlds, the Most Merciful, the Guider of hearts, the Provider of sustenance, the Owner of life and death.

Secondly, I would like to thank my respected supervisor, Dr. Mohammad Abdur Rashid, for his constant support and guidance to complete my project work properly. During the period of this project, he always shows me invaluable confidence.

I am also thankful to the authors of different publications (included in the bibliography), from where I have collected many supplementary pieces of information. Also, my gratitude goes to all faculty members of the department of physics for much helpful decision- making at different times.

On a personal note, I would like to thank my worshipful parents for their sacrifice and support over the years. Their love and encouragement always gives me mental support to continue my study smoothly.

Contents

List of Figures

List of Tables

Electronic and optical properties of pristine and Nb doped TiO_2: A DFT study

Chapter 1

Introduction

Titanium dioxide conjointly called titanium (IV) compound also called Titania belongs to the family of transition metal oxides, formula TiO_2 [1]. It has been widely studied, thanks to its fascinating general properties in a wide range of fields together with chemical change, photo-catalysis, and medication agents that have an effect on the standard of life. TiO_2 has been famed as a semiconductor with photo-catalytic activities and incorporates a pleasant potential for applications like dye hypersensitive cell [2, 3], environmental purification [4, 5] and nano-fluid applications [6, 7]. It's principally utilized in the shape of nanoparticles in suspension for top chemical action extent and activity [9]. Being a photo-catalyst material, TiO_2 has been necessary for numerous serious environmental and pollution challenges [10]. Pigment nanoparticles are bright with a high index of refraction ($\eta = 2.4$) that makes them appropriate for trade addressing dentifrice; reducing the toxicity of dyes and pharmaceutical drugs; wastewater treatment; copy of silkworm; area applications; coatings, papers, inks, plastics, food product, cosmetics, and textile. 3 crystalline phases of titanic oxide, are anatase (tetragonal), rutile (tetragonal), and brookite (orthorhombic) during which brookite has no industrial price. Thanks to their self-improvement and antifogging property, they're employed in the preparation of cloths, windows, tiles, and anti-fogging automobile mirrors. TiO_2 nanoparticles conjointly function surroundings sanitizing agent. The applications of nanoparticles synthesized by biological approach are going to be advantageous for the industries; surroundings and agriculture. The biogenesis of titanic oxide nanoparticles has gained wide interest among researchers thanks to its price effective, eco-friendly, and duplicatable

approach. The sol-gel route remedy of the titanic oxide from the surroundings is a vital step and it is often achieved by victimization physical processes like geological phenomenon and filtration.

The biogenesis of titanic oxide nanoparticles is often employed in comparison to chemical synthesis. The anatase and mineral structure are the foremost vital phases for TiO_2. Their optical, electrical, and structural properties are often measured with varied methodology however their theoretical investigation takes place in terms of density-functional-theory (DFT) approaches. Thanks to its achromatic color and robust interesting capabilities of actinic ray, TiO_2(rutile) has been used as a sun blocker. It's conjointly accustomed to building magnetism semiconductors (at high temperatures). It has enormous potential for spintronic applications. Therefore, researchers have studied it intensively to know its chemical and physical properties and to search out a lot of applications in varied fields. To perform our calculation we use FP-LAPW method within the DFT [12, 13], as implemented in WIEN2k package [53]. To do our calculation we use the mBJ approximation [14, 15] as the exchange-correlation potential. For comparison we also use GGA (PBE version) [16] approximation.

From the 19th century, DFT is the mainstay in the calculation of electronic structure in solid-state physics. Because this theorem uses approximate functionals (function of a function) which maintains the balance between accuracy and a computational result of a given problem. The problems which we can not solve analytically, we use computers and numerical methods to solve. DFT had started its journey in 1926 with Thomas-Fermi's theory. But present days DFT is not the same. The modern DFT was born in 1965 with Kohn- Sham equation. By introducing orbitals, they get 99 percent of the kinetic energy right to get accurate $n(r)$ and only need to approximate a small contribution. In the same year, Kohn-Sham also suggests Local Density Approximation (LDA) and Gradient expansion approximation. In 1993, more modern functionals (such as GGA and hybrids) are found to be usefully correct for thermochemistry. For the contribution in DFT, in 1998, Kohn and Pople win the Noble prize in Thermochemistry. After that DFT is used in material science, geology, soil science, astrophysics, protein folding, etc. It is mostly used in finding the electronic and optical properties of a many-body system.

In this report, we start by introducing TiO_2 in the first chapter. In this chapter, we have discussed what is TiO_2, What is its importance, and why we are investigating it. In chapter 2 we discussed the basic quantum mechanics which begins with the wave function. This

section contains the article about electron density, Schorödinger equation, time-dependent and independent Schrödinger equation, Hartree Fock approach, and its limitations.
Chapter 3 contains the theoretical investigation of Density Functional Theory (DFT). We start with the many-body quantum system then reduce it with the Born-Oppenheimer approximation. We have discussed Thomas-Fermi Dirac approximation, Hohenberg- Kohn Theorem, Spin density functional theorem, GGA, LDA+U method, Kohn-Sham equation, and how the Kohn-Shan equation can be solved. In chapters 4 and 5, the calculation part of this project is presented. Firstly we find the structural and optical properties of TiO_2. Then we doped it with 25% Nb and calculate its properties which we present in chapter 5. We calculate the Bandstructure, The Density of State and Optical properties of TiO_2 and Nb-doped TiO_2. We have done the volume optimization calculation, energy convergence analysis, and Spin polarization calculation of Nb-doped rutile TiO_2. And in chapter 6 we discussed the overall summary of this report.

Chapter 2

Basic Quantum Mechanics

2.1 Schrödinger equation

In 1920, Erwin Schrödinger describe the 'matter wave', where de Broglie's relations are used to describe plane waves hypothetically. Which gives the simplest Schrödinger equation which is called time-dependent Schrödinger equation [20].

$$i\hbar\frac{\partial}{\partial t}\Psi(\vec{r},t) = \hat{H}\Psi(\vec{r},t) \tag{2.1}$$

For a single particle,

$$\hat{H} = \hat{T} + \hat{V} = -\frac{\hbar^2}{2m}\vec{\nabla}^2 + V(\vec{r},t) \tag{2.2}$$

Where $\hat{H}$ is the Hamiltinoan, $\hat{T}$ is the kinetic energy term and $\hat{V}$ represents the potential energy term. And the equation represents the time dependent Schrödinger equation.

$$i\hbar\frac{\partial}{\partial t}\Psi(\vec{r},t) = [-\frac{\hbar^2}{2m}\vec{\nabla}^2 + V(\vec{r},t)]\Psi(\vec{r},t) \tag{2.3}$$

For N particle in three dimensional space, the Hamiltonian becomes

$$\hat{H} = \sum_{i=1}^{N}\frac{\hat{p}_i^2}{2m_i} + V(\vec{r}_1,\vec{r}_2,....\vec{r}_N,t) = -\frac{\hbar^2}{2}\sum_{i=1}^{N}\frac{1}{m_i} + V(\vec{r}_1,\vec{r}_2,....\vec{r}_N,t) \tag{2.4}$$

So the Schrödinger equation can be written in the form of

$$i\hbar\frac{\partial}{\partial t}\Psi(\vec{r}_1,\vec{r}_2,....\vec{r}_N,t)=[-\frac{\hbar^2}{2}\sum_{i=1}^{N}\frac{1}{m_i}\nabla_i^2+V(\vec{r}_1,\vec{r}_2,....\vec{r}_N,t)]\Psi(\vec{r}_1,\vec{r}_2,....\vec{r}_N,t) \tag{2.5}$$

2.2 Time independent Schrödinger Equation

We know the simplest time dependent Schrödinger equation is

$$\hat{H}\psi(\vec{r}_1,\vec{r}_2,....\vec{r}_N,t)=E\psi(\vec{r}_1,\vec{r}_2,....\vec{r}_N,t) \tag{2.6}$$

The above equation can be written in the form of,

$$\Psi(\vec{r}_1,\vec{r}_2,....\vec{r}_N,t)=\psi(\vec{r}_1,\vec{r}_2,....\vec{r}_N)\tau(t)=\psi(\vec{r}_1,\vec{r}_2,....\vec{r}_N).e^{-i\omega t} \tag{2.7}$$

By seperating the spatial and temporal part [21] of the wave function (using seperation of variables method) we get,

$$\hat{H}\psi(\vec{r}_1,\vec{r}_2,....\vec{r}_N)=E\psi(\vec{r}_1,\vec{r}_2,....\vec{r}_N) \tag{2.8}$$

This is the general Eigenvalue equation. The solution of the time independent Schrödinger equation represents the standing wave which also called stationary wave. Time independent Schrödinger equation is more easier to solve than the time dependent equation.
Using many body Hamiltonian, the Schrödinger equation becomes,

$$[-\frac{\hbar^2}{2}\sum_{i=1}^{N}\frac{1}{m_i}\nabla_i^2+V(\vec{r}_1,\vec{r}_2,....\vec{r}_N)]\Psi(\vec{r}_1,\vec{r}_2,....\vec{r}_N)=E\psi(\vec{r}_1,\vec{r}_2,....\vec{r}_N) \tag{2.9}$$

Where the Hamiltonian itself has no time depedency. So the potential is also time independent.

2.3 Wave function

We know that the first and formost postulate of basic quantum mechanics is that "the state of a particle is compleatly described by it's wave function(time independent)", that is, the wave function contains all the necessary informations about a particle's state. Quantum

mechanically it is denoted by Ψ. Basically it has no physical meaning. The square of it's modulas gives the probability of finding a particle in a given region. The properties of a valid wave function are:

In order to avoid infinity probabilities, ψ must be finite everywhere. In order to avoid multiple values of the probability ψ must be single valued. For finite potentials, ψ and $\frac{\partial\psi}{\partial x}$ must be continious. This is required because the second order derivative term in the wave equation must be single valued.(There are exceptions to this rule when V is infinity). In order to normalize the wave functions, ψ must approach zero as x approaches $\pm\infty$ The motion of Quantum particle can be explained with Ψ when operated with Schrödinger Equation. The product of Ψ^* and Ψ represent the probability density function [17,19]. Where Ψ^* is called the complex conjugate of Ψ. The probability of finding a particle in whole space is unity. That is,

$$\int \Psi\Psi^* dv = 1 \tag{2.10}$$

This is called normalization condition. Wave function must be continious over the full spatial range and square-integratable. [18]

2.4 The Many-Body System and Born-Oppenheimer Approximation

In case of a many body system containing nucli and electrons, tha Hamiltonian can be written as,

$$H_{tot} = -\sum_I \frac{\hbar^2}{2m_I}\nabla^2_{R_I} - \sum_i \frac{\hbar^2}{2m_e}\nabla^2_{r_i} + \frac{1}{2}\sum_{\substack{I,J \\ I\neq J}} \frac{Z_1 Z_J e^2}{|R_I - R_J|} + \frac{1}{2}\sum_{\substack{i,j \\ i\neq j}} \frac{e^2}{|r_i - r_j|} - \sum_{I,i} \frac{Z_1 e^2}{|R_I - r_i|} \tag{2.11}$$

The first term $\sum_I \frac{\hbar^2}{2m_I}\nabla^2_{R_I}$ of the above equation represents the kinetic energy of the Nucli. Second term $\sum_i \frac{\hbar^2}{2m_e}\nabla^2_{r_i}$ represents the kinetic energy of the electrons. Third term $\frac{1}{2}\sum_{\substack{I,J \\ I\neq J}} \frac{Z_1 Z_J e^2}{|R_I - R_J|}$ is for the potential energy of nucli- nucli coulonb interaction. Fourth term $\frac{1}{2}\sum_{\substack{i,j \\ i\neq j}} \frac{e^2}{|r_i - r_j|}$is for the potential energy of electron electron coulomb interaction and the last term $\sum_{I,i} \frac{Z_1 e^2}{|R_I - r_i|}$ represents the potential energy of nucli- electron coulomb interaction.

For a system, time independent Schrödinger equation becomes,

$$H_{tot}\Psi(\{R_I\}\{r_i\}) = E\Psi(\{R_I\}\{r_i\}) \tag{2.12}$$

where,

$\Psi(\{R_I\}\{r_i\})$= total wave function of the system. The solution of this equation gives us a 2^{nd} order differential equation which is still impossible to solve. So in 1927, a so called approximation was made by Born and Oppenheimer [23]. As we know the nucli is slower and heavier than the electrons. We can seperate the movement of electrons and nucluos. When the nucli is considered to be fixed the total Ψ can be written as,

$$\Psi(\{R_I\}\{r_i\}) = \Theta(\{R_I\})\phi(\{r_i\}\{R_I\}) \tag{2.13}$$

where,

$\Theta(\{R_I\})$ = position of the nucli

$\phi(\{r_i\}\{R_I\})$= position of the electrons

With Born- Oppenheimer approximation equation 2.12 can be written as,

$$H_e\Phi(\{r_i\}\{R_I\}) = V(\{R_I\})\phi(\{r_i\}\{R_I\}) \tag{2.14}$$

where,

$$H_e = -\sum_i \frac{\hbar^2}{2m_e}\nabla^2_{r_i} + \frac{1}{2}\sum_{\substack{I,J \\ I\neq J}} \frac{Z_1 Z_J e^2}{|R_I - R_J|} + \frac{1}{2}\sum_{\substack{i,j \\ i\neq j}} \frac{e^2}{|r_i - r_j|} - \sum_{I,i} \frac{Z_1 e^2}{|R_I - r_i|} \tag{2.15}$$

and

$$[-\sum_I \frac{\hbar^2}{2m_I}\nabla^2_{R_I} + V(\{R_I\})]\theta(\{R_I\}) = E'\theta(\{R_I\}) \tag{2.16}$$

The eigenvalues of $V(\{R_I\})$ depends on the position of the nucli. By solving equation 3.5 we can find V and putting this in above equation motion of the nucli can be obtained.

The importance of Born- Oppenheimer approximation is the seperation of the movement of the nucli and electrons. Now we can take the electrons moving in a static external potential $V_{ext}(r)$ formed by the nucli, which is the starting point of DFT.

2.5 Hartree-Fock approach

The Hartree-Fock (HF) approach is the first standard approach to many body system which was applied in 1930 by Fock to atoms. The problems which are not possible to solve analitycally of many body problems, this theory gives a suitable strategy to approximate it. It is as similar as the Least Action Principle (Classical Mechanics).

For now we have the interest only on the electronic schrö dinger equation. Therefore we get, $\hat{H} \equiv H_{el}, \hat{E} \equiv E_{el}$.

The energy (observable) correspond to the general Hamiltonian operator can be calculated as,

$$E =< \hat{H} >= \int d\vec{r}_1 \int d\vec{r}_2 ... \int d\vec{r}_N \psi^*(\vec{r}_1, \vec{r}_2, ...\vec{r}_N)\hat{H}\psi(\vec{r}_1, \vec{r}_2, ...\vec{r}_N) \tag{2.17}$$

If we take a wave function as a trial, the energy obtained is not the same as the actual ground state wave function. Actual ground state energy is always lower than the obtained energy. If trial wave function is equal as the ground state wave function, the energies in both cases are equal.

$$E_{trial} \geq E_o \tag{2.18}$$

with

$$E_{trial} = \int d\vec{r}_1 \int d\vec{r}_2 ... \int d\vec{r}_N \psi^*_{trial}(\vec{r}_1, \vec{r}_2, ...\vec{r}_N)\hat{H}\psi_{trial}(\vec{r}_1, \vec{r}_2, ...\vec{r}_N) \tag{2.19}$$

and

$$E_o = \int d\vec{r}_1 \int d\vec{r}_2 ... \int d\vec{r}_N \psi^*_o(\vec{r}_1, \vec{r}_2, ...\vec{r}_N)\hat{H}\psi_o(\vec{r}_1, \vec{r}_2, ...\vec{r}_N) \tag{2.20}$$

With Dirac's Bra-ket notation [22], above equation can be written as,

$$\langle\psi_{trial}|\hat{H}|\psi_{trial}\rangle = E_{trial} \geq E_o = \langle\psi_o|\hat{H}|\psi_o\rangle \tag{2.21}$$

2.6 Limitations of Hartree-Fock approach

When the even number of electrons are located in double occupied spatial orbital, it is called that the compound is in singlet state. It also called closed-shell system. Again having odd number of electrons (compound with single occupied orbital) is called triplet state. It also called open shell system. This two types of system gives us two different approaches of

Hartree-Fock methood.

In restricted HF (RHF) methood, all electrons are considered to be paired where as in UHF method, this restriction is lifted totally.

The size of the investigated system is a limiting factor for calculation. Kohn states M=p^5 with $3 \leq p \leq 10$ parameters for the result with sufficient accuracy in investigation of H_2 system. For N=100,

$$M = p^{3N} = 3^{300} to 10^{300} \approx 10^{150} to 10^{300} \tag{2.22}$$

Above equation states that, the minimization of energy would have to be performed at least 10^{150} dimension. HF method are restricted to systems with small number of electrons.

Chapter 3

Density Functional Theory (DFT)

3.1 Thomas-Fermi approximation

The original DFT in quantum system is the method of Thomas [24] and Fermi [25] which was proposed in 1927. But their approximation was not accurate enough for todays electronic structure determination. The kinetic energy of the system of electrons was approximated as the explicit functional of density and taken as non-interactive electron in a homogeneous gas with equal density to local density at any given point. Exchange and correlation among electrons was nglected in Thomas and Fermi model.

In 1930, it was extended by Dirac [26] which is still in use today. This drives to the energy functional for electrons in an external potential $V_{ext}(r)$

$$E_{TF}[n] = C_1 \int d^3r n(r)^{5/3} + \int d^3 V_{ext} n(r) + C_2 \int d^3r n(r)^{4/3} + 1/2 \int d^3r d^3r' \frac{n(r)n(r')}{|(r-r')} \quad (3.1)$$

where the first term is the local approximation to the kinetic energy with $C_1 = \frac{3}{10}(3\pi^2)^{2/3} = 2.871au$, the third term is the local exchange with $C_2 = -\frac{3}{4}(\frac{3}{\pi})^{1/3}$ and the last term is the classical electrostatic Hartree energy.

The ground state density and energy can be written as,

$$\int d^3r n(r) = N \quad (3.2)$$

The solution of above equation can be found as, (using the methood of Lagrange Multiplier)

$$\Omega_{TF}[n] = E_{TF}[n] - \mu \int d^3 r n(r) - N \tag{3.3}$$

Where, μ =Lagrangian multiplier, which denotes the Fermi energy. For small variations in density $\delta n(r)$, the condition for stationary point is,

$$\int d^3 r(\Omega_{TF}[N(r) + \delta n(r)] - \Omega_{TF}[n(r)]) \rightarrow \int d^3 r(\frac{5}{3} C_1 n(r)^{2/3} + V(r) - \mu)\delta n(r) = 0 \tag{3.4}$$

where $V(r) = V_{ext}(r) + V_{Hartree}(r) + V_x(r)$ is the total potential. From the above equation the functional is stationary if and only if the potential and density satisfies the relation

$$\frac{1}{2}(3\pi^2)^{2/3} + V(r) - \mu = 0 \tag{3.5}$$

The density functional theory is attractive because of the fact that one equation for the density is simplier than the many body Schrödinger equation which contains 3N degrees of freedom for N electrons. The approximation with which the Thomas-Fermi approach starts that are too crude, essential chemistry and physics are missing such as binding of nucleus and shell structures of atoms etc. Thus it fails to reach the goal of a useful description of electrons in matter.

3.2 Hohenberg-Kohn Theorem

The formulation of density functional theory as an exact theory of many body system was the approach of Hohenberg and Kohn [27]. As we all know, the ground state energy and ground state wave function can be determined by minimizing $E|\psi|$ (energy functionals) for an electronic system described by the Hamiltonian. But in case of many electron system(N electron) N and v(r) describe all the properties for ground state. The discussion in this report is confined only for non degenerate ground state. The theory is based upon two theorems.

3.2.1 Theorem 1

Statement : The ground state energy E is a unique functional of the electron density.

$$E = E[n(r)] \tag{3.6}$$

Proof: We know that the ground state particle density is n(r) for a system and $V_{ext}(r)$ is the external potential for the system. The proof is based on minimum energy principle. Suppose we have different two potential $V_{ext}(r)$ and $V'_{ext}(r)$, which is different from each other by a constant but lead to the same ground state density $n_0(r)$ For that we will get the different Hamiltonian H and H' and different ground state wave functions.

$$\hat{H}\Psi = E_0\Psi \tag{3.7}$$

$$\hat{H}'\Psi' = E'_0\Psi' \tag{3.8}$$

Since Ψ' is not the ground state of $\hat{H}$. It follows that

$$E_0 < \langle\Psi'|\hat{H}|\Psi'\rangle \tag{3.9}$$

$$< \langle\Psi'|\hat{H}'|\Psi'\rangle + \langle\Psi'|\hat{H} - \hat{H}'|\Psi'\rangle \tag{3.10}$$

$$< E'_0 + \int n_0(r)[V_{ext}(r) - V'_{ext}(r)]dr \tag{3.11}$$

Similarly,

$$E'_0 < \langle\Psi|\hat{H}'|\Psi\rangle \tag{3.12}$$

$$< E_0 + \int n_0(r)[V'_{ext}(r) - V_{ext}(r)]dr \tag{3.13}$$

By adding equation 3.17 and 3.19 we get,

$$E_0 + E'_0 < E'_0 + E_0 \tag{3.14}$$

As the Hamiltonian is fully known, except for a constant shift of energy, it says that the many body wavefunction for all state are determined. Therefore all the properties of the

system are completely determined if and only if the ground state density is known. [28]

3.2.2 Theorem 2

Statement: If the functional $E[n(r)]$ is known, the exact ground state energy and density can be fully determined.

Proof: The Universal functional can be written as,

$$F[n(r)] \equiv \hat{T}[n(r)] + E_{int}[n(r)] \tag{3.15}$$

where,
$\hat{T}[n(r)]$ = kinetic energy
$E_{int}[n(r)]$ = interaction energy of the particles
The energy functional $E[\Psi']$ (according to variational principle)

$$E[\Psi'] \equiv \langle \Psi' | \hat{T} + \hat{V}_{int} + \hat{V}_{ext} | \Psi' \rangle \tag{3.16}$$

When $\Psi' = \Psi_0$, it has a global minimum value with a constant that the total number of particles are conserved. According to HK theorem 1 Ψ' must correspond to the ground state whose particle densityis $n'(r)$ and external potential is $V'_{ext(r)}$. Then $E[\psi']$ is a functional of $n'(r)$. According to the variational principle,

$$\begin{aligned} E[\Psi'] &\equiv \langle \Psi' | \hat{T} + \hat{V}_{int} + \hat{V}_{ext} | \Psi' \rangle && (3.17)\\ &= E[n'(r)] && (3.18)\\ &= \int n'(r) V'_{ext}(r) dr + F[n'(r)] && (3.19)\\ &> E[\psi_0] && (3.20)\\ &= \int n_0(r) V_{ext}(r) dr + F[n_0(r)] && (3.21)\\ &= E[n_0(r)] && (3.22) \end{aligned}$$

Hence, Energy functional $E[n(r)] \equiv \int n_0(r) V_{ext}(r) dr + F[n_0(r)]$ evaluats for the correct ground state density $n_0(r)$ is lower than the value of the function of any other density n(r). By minimizing the total energy functional with respect to the variations in the density n(r), one could find the exact ground state density and energy. [29]

3.3 Kohn-Sham Equation

Hohenberg and Kohn framework is not very usefull yet in actual calculation. The second Hohenberg-Kohn theorem is the only possibility for the minimization of energy. An example of an iterative approachis the Hartree equation for self consistent single particle [38,39]. The Hartree equation is clearly a wavefunction based equation and it is not directly related to Hohenberg and Kohn. Hartree's approximation says that every electron moves in an effective single particle potential of the form of,

$$v_H(\vec{r}) = -\frac{Z}{|\vec{r}|} + \int \frac{n(\vec{r})}{|\vec{r} - \vec{r'}|} d\vec{r} \tag{3.23}$$

where,

$-\frac{Z}{|\vec{r}|}$= attractive coulomb potential of a nucleus with an atomic number Z.

$\int \frac{n(\vec{r})}{|\vec{r}-\vec{r'}|} d\vec{r}$ = correspond to the potential caused by the mean electron density distribution $n(\vec{r})$.

$n(\vec{r})$ can be expressed in terms of the single particle wave functions,

$$n(\vec{r}) = \sum_{j=1}^{M} |\phi_j(\vec{r})|^2 \tag{3.24}$$

According to the Pauli exclusion principle, the sum of above equation runs over the lowest eigenvalues. For single particle, 3N-dimensional Schrödinger equation can be written as,

$$[-\frac{1}{2}\vec{\nabla}^2 + v_H(\vec{r})] \qquad \phi_j(\vec{r}) = \epsilon_j \phi_j(\vec{r}) \qquad j = 1, ..., N \tag{3.25}$$

Therefore Khon and Sham investigated the DFT applied to a system of N non-interacting electrons in an external potential. The expression for the energy of such a system is,

$$E_{v(\vec{r})}[n'(\vec{r})] \equiv \int v(\vec{r}) n'(\vec{r}) d\vec{r} + T_s[n'(\vec{r})] \geq E \tag{3.26}$$

where,

$n'(\vec{r})$ = v respectable density for non interacting electrons

$T_s[n'(\vec{r})]$= kinetic energy of the ground state of those non-interacting electron [38]

In case of non-interacting electron, the Euler-Lagrange equation [40] can be written as,

$$\delta E_v[n'(\vec{r})] \equiv \int \delta n'(\vec{r})[v(\vec{r}) + \frac{\delta}{\delta n'(\vec{r})} T_s[n'(\vec{r})]|_{n'(\vec{r})=n(\vec{r})} - \epsilon] d\vec{r} = 0 \tag{3.27}$$

where,

$n'(\vec{r})$= exact ground state density for the potential $v(\vec{r})$

ϵ= The Lagrangian multiplier to ensure particle density conservation.

For such a system the total ground state energy and particle density can simply be written as,

$$E = \sum_{j=1}^{N} \epsilon_j \tag{3.28}$$

and

$$n(\vec{r}) = \sum_{j=1}^{N} |\phi_j(\vec{r})|^2 \tag{3.29}$$

For an interacting case the construction of Eular-Lagrange equation becomes,

$$\delta E_v[n'(\vec{r})] \equiv \int \delta n'(\vec{r})[v_{eff}(\vec{r}) + \frac{\delta}{\delta n'(\vec{r})} T_s[n'(\vec{r})]|_{n'(\vec{r})=n(\vec{r})} - \epsilon] d\vec{r} = 0 \tag{3.30}$$

with

$$v_{eff}(\vec{r}) \equiv v(\vec{r}) + \int \frac{n(\vec{r})}{|\vec{r} - \vec{r}'|} d\vec{r} + v_{xc}(\vec{r}) \tag{3.31}$$

and the functional derivative

$$v_{xc}(\vec{r}) \equiv \frac{\delta}{\delta n'(\vec{r})} E_{xc}[n'(\vec{r})]|_{n'(\vec{r})=n(\vec{r})} \tag{3.32}$$

The corresponding equations are the single particle Schrödinger equation

$$[-\frac{1}{2}\vec{\nabla}^2 + v_{eff}(\vec{r})] \qquad \phi_j(\vec{r}) = \epsilon_j \phi_j(\vec{r}) \qquad j = 1, ..., N \tag{3.33}$$

As well as the equation for the particle density is

$$n(\vec{r}) = \sum_{j=1}^{N} |\phi_j(\vec{r})|^2 \tag{3.34}$$

Which form together self consistent Khon -Sham equation and effective potential. If one use the exact $E_{xc}[n(\vec{r})]$ and $v_{xc}[n(\vec{r})]$ it would be possible to find the exact solution.

3.4 Solving Kohn-Sham equation

In a condensed matter system the KS equation gives a way to obtain the exact density and energy of the ground state. The process starts with an initial electron density n(r), usually a superposition of atomic electron density, then the effective KS potential V_{KS} is calculated and the KS equation is solved with single-particle eigenvalues and wavefunctions, a new electron density is then calculated from the wavefunctions.

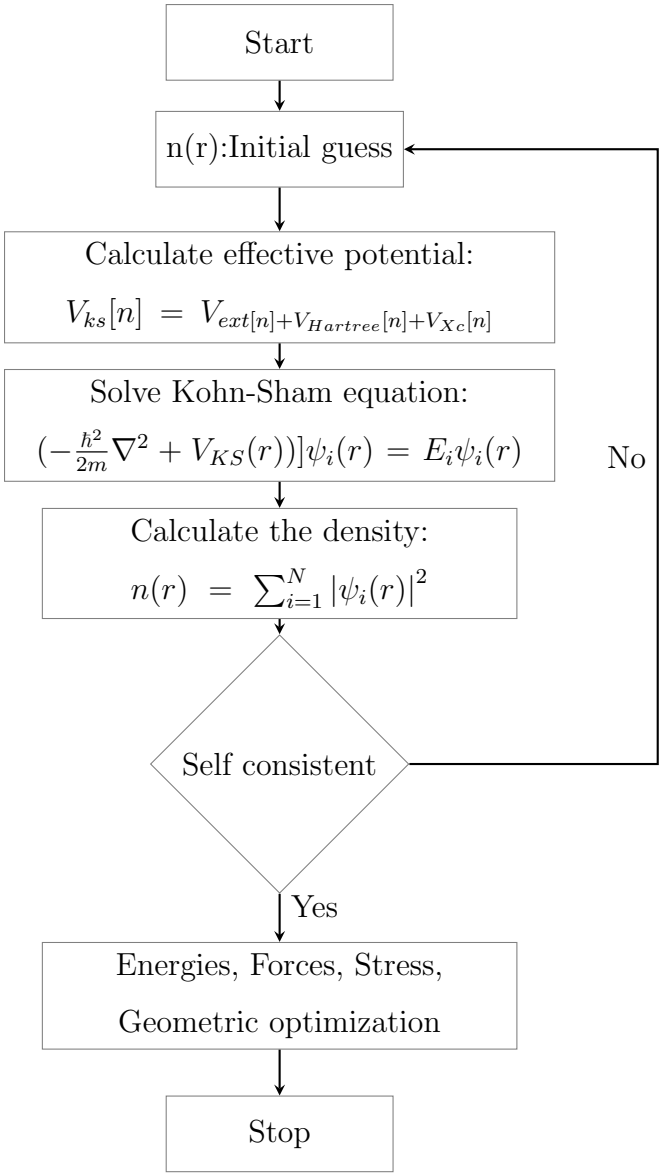

This is usually done numerically through some self consistent iteration as shown in above flowchart . Self-consistent condition(s) can be the change of total energy or electron density

from the previous iteration or total force acting on atoms is less than some chosen small quantity, or a combination of these individual conditions. If the self-consistency is not achieved, the calculated electron density will be mixed with electron density from previous iterations to get a new electron density. A new iteration will start with the new electron density. This process continues until self-consistency is reached. After the self-consistency is reached, various quantities can be calculated including total energy, forces, stress, eigenvalues, electron density of states, band structure, etc..

3.5 Generalized-Gradient Approximations

The LSDA neglects inhonogeneities of real charge density which could be defferent from the Homogeneous Electron Gas(HEG). The exchange correlation energy density has significantly defferent result from HEG. This gives rise to the various Generalized-Gradient Approximations (GGA) which include density gradient correlation and higher spatial dertiviatives of electron density and gives better result than LDA in many cases. Three most widely used GGA'S are the from propeosed by Becke [30], Perdew et al. [31]and Perdew, Burke and Enzerhof [32]. From spin polarized system [33] we know that:

$$E_{XC}^{LSDA} \qquad [n_\uparrow(r), n_\downarrow(r)] = \int n(r) \qquad \epsilon_{XC}^{hom}(n_\uparrow(r), n_\downarrow(r))dr \tag{3.35}$$

Where XC energy density $\epsilon_{XC}^{hom}(n(r))$ is a function of the density alone and is decomposed into exchange energy density $\epsilon_X^{hom}(n(r))$ and correlation energy density $\epsilon_C^{hom}(n(r))$. So that the XC energy functional is decomposed into exchange energy functional $E_X^{LDA}[n_(r)]$ and correlation energy functional $E_C^{LDA}[n_(r)]$ linearly.
From density gradient $\nabla n(r)$,

$$E_{XC}^{GGA} \qquad [n_\uparrow(r), n_\downarrow(r)] = \int n(r) \qquad \epsilon_{XC}^{hom}(n_\uparrow(r), n_\downarrow(r), |\nabla n_\uparrow(r)|, |\nabla n_\downarrow(r)|, ...)dr \tag{3.36}$$

$$= \int n(r) \qquad \epsilon_X^{hom} n(r))F_{XC}(n_\uparrow(r), n_\downarrow(r), |\nabla n_\uparrow(r)|, |\nabla n_\downarrow(r)|, ...)dr \tag{3.37}$$

Where F_{XC} is dimensionless and $\epsilon_X^{hom} n(r))$ is the exchange energy density of the unpolarized HEG. F_{XC} can be decomposed linearly into exchange contribution F_c as $F_{XC} = F_x + F_c$.
Generally GGA works better than LDA, in pridicting binding energy of molecules and bond length, crystall lattice constants, especially the system where charge density varried rapidly.

In case of ionic crystall, GGA overcorrects LDA results where the lattice constants of LDA fit well than GGA. But in case of transition metal oxides and rare-earth element, both LDA and GGA parform badly. This drawback leads to approximations beyond LDA and GGA.

3.6 Local Spin Density Approximation (LSDA)

Spin DFT is important in the theory of atoms amd molecules with net spins, as well as solids with magnetic order. The relevent example for our purpose is the Zeeman term that is different Fermions with up and down spin. According to this model the particle density,

$$n(r) = n(r, \sigma =\uparrow) + n(r, \sigma =\downarrow) \tag{3.38}$$

and the spin density

$$s(r) = n(r, \sigma =\uparrow) - n(r, \sigma =\downarrow) \tag{3.39}$$

This results the energy density as

$$E = E_{HK}[n, s] \equiv E'_{HK}[n] \tag{3.40}$$

Where [n] denotes the functionl of the density which depends both on space and spin. In absance of external Zeeman fields, the soluton of lowest energy may be spin polarized. That is,

$$n(r, \sigma =\uparrow) \neq n(r, \sigma =\downarrow) \tag{3.41}$$

which is anologous to the broken symmetry solution of unrestricted Hartree-Fock theorem. The usefulness of spin Density Functional Theory is in these cases as well. The original Hartree-Fock theorem are valid and the ground state is determined by total ground state density $n(r, \sigma =\uparrow) + n(r, \sigma =\downarrow)$ for the system where there is no spin dependent external potential.

3.7 LDA+U Method

The systems which are strongly correlated contain rare-earth metal (transition metal) having partially filled d or f shells. L(S)DA and GGA can not explain them properly. In this method, electrons are considered into two classes: delocalized s, p electron and localized d

or f electrons. The total energy in L(S)DA+U [34] method is given by,

$$E_{tot}^{LDA+U}[\rho_\sigma(r), \{n_\sigma\}] = E^{LSDA}[\rho_\sigma(r)] + E^{U}[\{n_\sigma\}] - E_{dc}[\{n_\sigma\}] \tag{3.42}$$

where,

σ = spin indexes

$\rho_\sigma(r)$ = electron density for spin-σ electrons

$\{n_\sigma\}$ = density matrix of f or d electron for spin-σ electrons

$E^{LSDA}[\rho_\sigma(r)]$ = standard LSDA energy functional

$E^{U}[\{n_\sigma\}]$ = electron-electron coulomb interaction energy . The last term is double counting term which remove the average LDA energy contribution of d or f electrons from the LDA energy

$$E_{dc}[\{n_\sigma\}] = \frac{1}{2}UN(N-1) - \frac{1}{2}J[N_\uparrow(N_\uparrow - 1) + N_\downarrow(N_\downarrow - 1)] \tag{3.43}$$

where,

$N = N_\uparrow + N_\downarrow$.

U and J are coulomb and exchange parameters. If exchange and non sphericity is neglected then,

$$E_{tot}^{LDA+U} = E_{LDA} + \frac{1}{2}U\sum_{i\neq j} n_i n_j - \frac{1}{2}UN(N-1) \tag{3.44}$$

The orbital energies ε_i are derivative of above equation with respect to orbital occupations n_i:

$$\varepsilon_i = \frac{\partial E}{\partial n_i} = \varepsilon_{LDA} + U(\frac{1}{2} - n_i) \tag{3.45}$$

For $n_i = 1$,LDA orbital energiesare shifted by $-\frac{U}{2}$ and by $\frac{U}{2}$ for unoccupied orbitals ($n_i = 0$) , resulting the upper and lower Hubbard bands, which opens a gap at the Fermi energy in transition metal oxides. In case of double counting term, it has two different tretement: AMF and FLL. The former is most suitable for small U system [35] and the letter for large U system [36]. The energies for double counting is given by [37],

$$E_{AMF}^{dc} = \frac{1}{2}UN^2 - \frac{U+2lJ}{2l+1}\frac{1}{2}\sum_{\sigma} N_{\sigma}^2 \tag{3.46}$$

and

$$E_{AMF}^{dc} = \frac{1}{2}UN(N-1) - \frac{1}{2}J\sum_{\sigma} N_{\sigma}(N_{\sigma-1}) \tag{3.47}$$

where,

$\frac{N}{2(2l+1)}$ = average occupation of the correlated orbitals

$\frac{N_{\sigma}}{2l+1}$ = average occupation of a single spin of the correlated orbital

Chapter 4

TiO_2: A test case

TiO_2 is a widely studied compound mainly have the three crystal types rutile, anatase, and brookite are found in nature. Only the first two play a significant part in artificial operations. Experimental data on TiO_2 brookite is limited due to its frequentness and delicate medication [41]. As a semiconductor material with long-term stability, non-toxic environmental adequacy, and astronomically low-cost vacuity TiO_2 has also been taken into account for photovoltaic operations. Still, due to optic gaps slightly above 3 eV (rutile: 3.0 eV [42,43], anatase: 3.4 eV [44] and brookite: 3.3 eV [45], natural TiO_2 is only photoactive in the UV region of the electromagnetic spectrum and an inefficient active solar cell material. Still, the material advantages of TiO_2 can be used laterally technically and economically. Feasible color-acclimatized solar cells where it acts as an electron-transporting substrate for a chemisorbed photoactive color.

4.1 Crystallographic Structure

According to atomic physics and quantum chemistry, crystallographic structure is the distribution of electrons of an atom or molecules in atomic or molecular orbitals. TiO_2 has two important phases, anatase and rutile and both of them are tetragonal in structure. Structure of TiO_2 rutile is shown in figure 4.1.

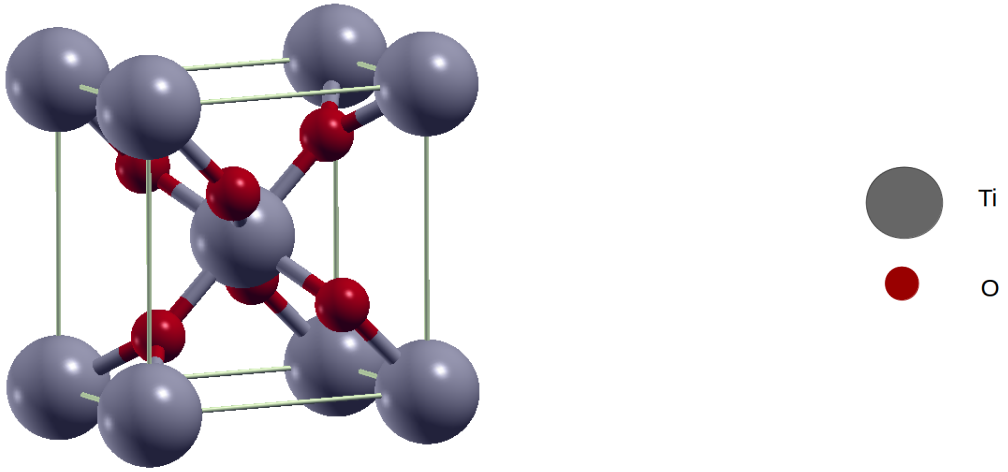

Figure 4.1: Crystallographic structure of TiO_2 rutile phase.

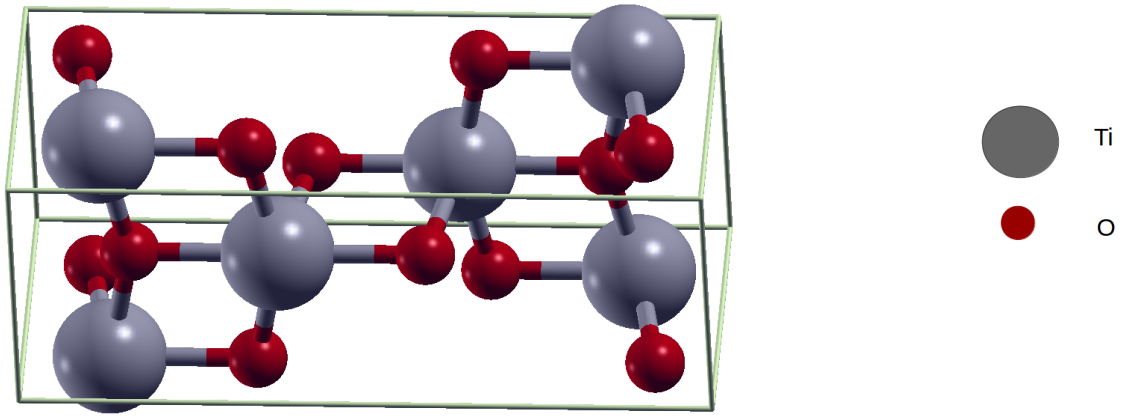

Figure 4.2: Crystallographic structure of TiO_2 anatase phase.

Structure of TiO_2 anatase is shown in figure 4.2. The parameters which are necessary to draw the electronic structure of TiO_2 rutile and anatase is given in table 4.1.

Table 4.1: Parameters needed to draw the electronic structure of rutile and anatase TiO_2.

Parameters	TiO_2 (Rutile)	TiO_2 (Anatase)
Lattice	$P4_2$/mnm (No.136)	$I4_1$/amd (No.141)
a	4.586	3.782
b	4.586	3.782
c	2.954	9.502
α, β, γ	90	90
Ti	0.5, 0.5, 0.5	0.5, 0.75, 0.375
O	0.1954, 0.8046, 0.5	0.5, 0.75, 0.1618

4.2 Self Consistent Field (SCF)

We perform the calculation with 1000 k-points in the first Brillouin zone for both rutile and anatase structure. Used R_{kmax} was 7. Mesh details for rutile is 8×8×13 and for anatase is 10×10×10. Energy convergence criteria was 0.00001 Ry and charge convergence criteria was 0.0001 e, where e is the charge of electron. The RMT values we use in calculation is given in table 4.2.

Table 4.2: RMT values used in the formation of rutile and anatase TiO_2 crystallographic structure.

Phase	Potential	RMT	
		Ti	O
Rutile	PBE	1.90	1.72
	mBJ	1.90	1.72
Anatase	PBE	1.84	1.66
	mBJ	1.84	1.66

RMT stands for Radius Muffin-Tin which describes the radious of the atoms we use. It is necessary to use appropriate RMT so that the atomic sphere of one atom must not be in touch with another. We have found the Band gap with PBE and mBJ apporimation is given in table 4.3. Both rutile and anatase bandstructure provides a direct band gap which means that both rutile and anatase are non-metalic in bahavior. Calculated total energy, Fermi energy, and magnetic moment for both structure is given in table 4.4.

Table 4.3: Estimated band gap for both rutile and anatase phase with PBE and mBJ approximation.

Phase	Band Gap (eV)	
	PBE	mBJ
Rutile	1.822	2.561
Anatase	1.977	2.817

Table 4.4: Total energy, Fermi energy and magnetic moment estimated from the SCF with PBE and mBJ potential for both anatase and rutile phase.

Phase	Potential	Total energy (eV)	Fermi energy (eV)	Magnetic Moment
Rutile	PBE	-4018.06676879	0.3682081574	0.00002
	mBJ	-4006.43935176	0.3997111379	0.0000
Anatase	PBE	-4018.07684582	0.3120134224	0.00007
	mBJ	-4006.39506933	0.3571528680	-0.00001

4.3 Energy convergence analization

Basically the energy convergence curve shows how many iterations are needed and how the energy is converged.

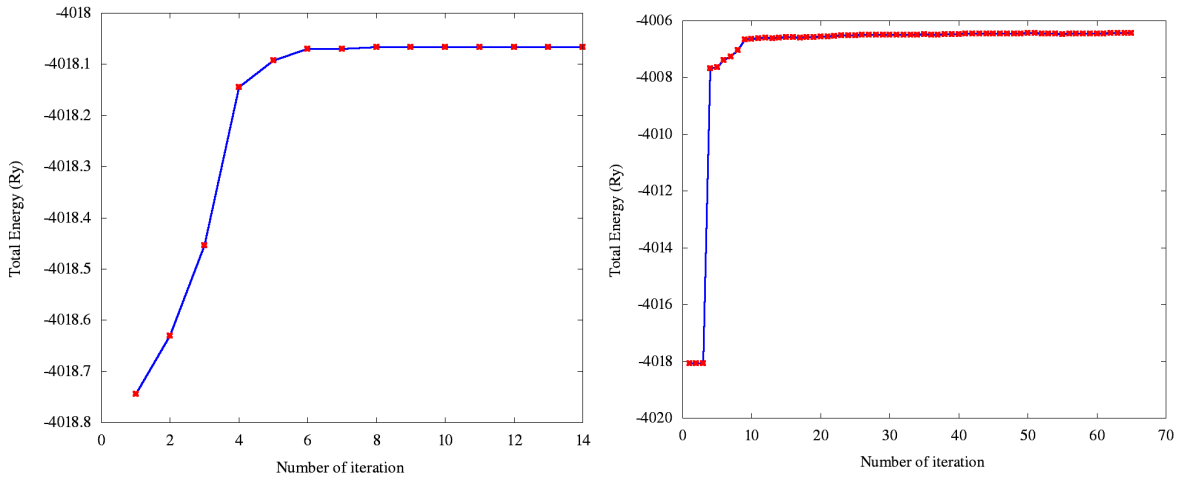

Figure 4.3: Energy convergence curve of rutile TiO_2. Left for PBE and right for mBJ approximation

If we make a comparison between anatase and rutile, anatase structure takes more iteration to converge the energy.

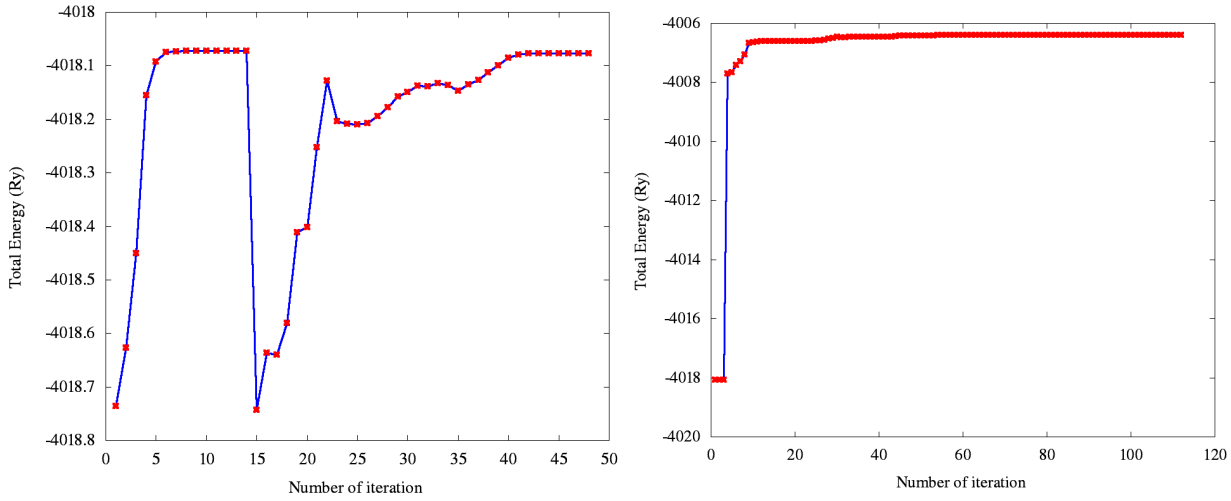

Figure 4.4: Energy convergence curve of anatase TiO_2. Left for PBE and right for mBJ approximation

4.4 Bandstructure

Figure 4.5 represents the bandstructure of rutile between -6 and 6 eV. It can be seen that the valance band maximum (VBM) and conduction band minimum (CBM) of the rutile are both at Γ point which then produces a direct bandgap. Bandgap for rutile with PBE

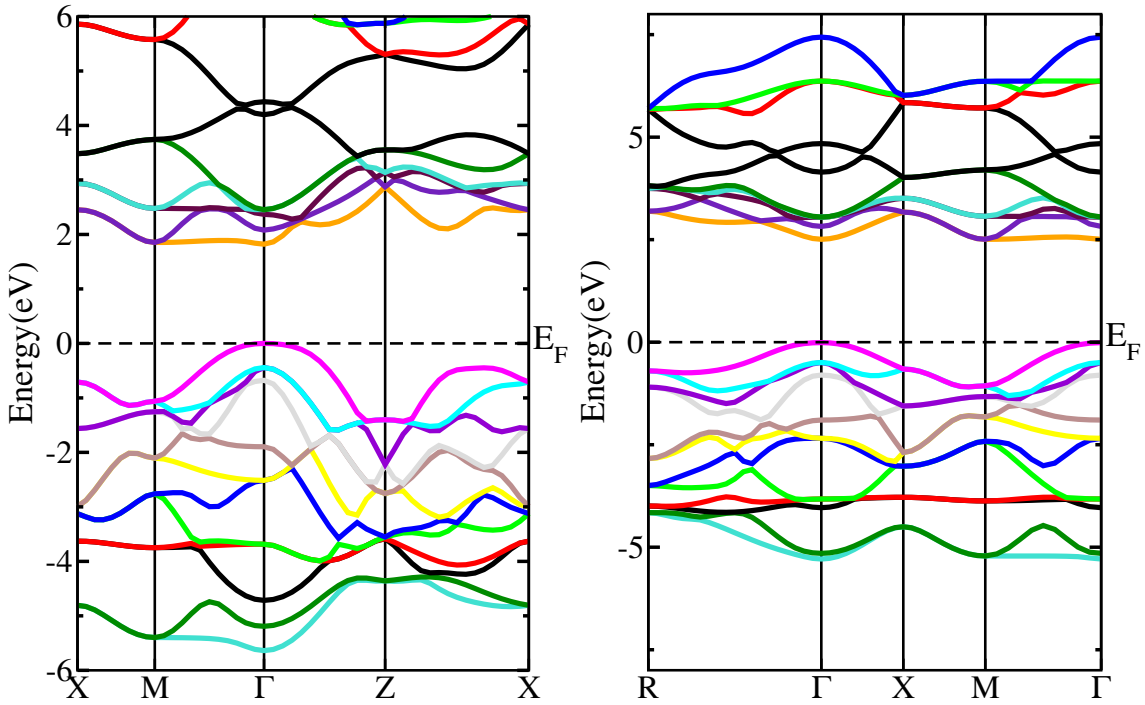

Figure 4.5: Estimated bandstructure of rutile phase with PBE (left) and mBJ (right) potential.

approximation is 1.822 eV and with mBJ it is 2.561 eV. Calculated values of widths of valance band for the rutile are approximately equivalent to 5.5 eV with an excellent agreement with

the experimental values of 5.4 eV [51]. Figure 4.6 represents the bandstructure of anatase between -6 and 8 eV. From the figure, we can see that the valance band maximum(VBM) and conduction band minimum (CBM) produces the direct bandgap. Bandgap found for anatase structure is 1.977 eV with PBE and 2.817 with mBJ approximation.

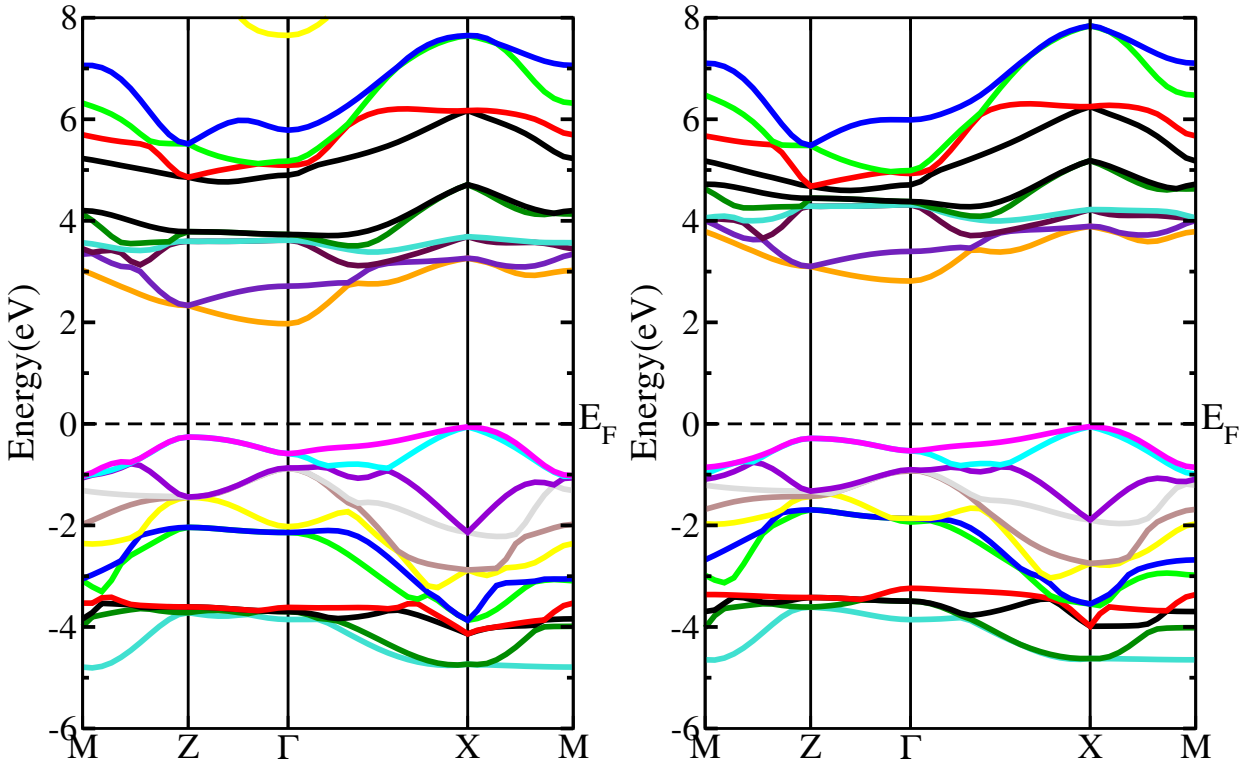

Figure 4.6: Estimated bandstructure of anatase phase. Left for PBE and right for mBJ potential.

Calculated values of widths of valance band for the rutile are approximately equivalent to 4.8 eV with an excillent agreement with the experimental values of 4.7 eV [52]. In both structure valance band is closer to the Fermi level than the conduction band.

4.5 Density of state

Figure 4.7 and 4.8 represent the total density of state(TDOS) and partial density of states (PDOS) for both up and down spin for rutile and anatase respectively. From figure 4.7, for anatase valence band ranges from 4.8 to 0 eV for PBE and 4.6 to 0 eV for mBJ approximation. The bandgap is 1.977 eV for PBE and 2.817 for mBJ approximation. The larger gap in the anatase is correlated with the narrower width of its valance bands and conduction bands in the energy window.

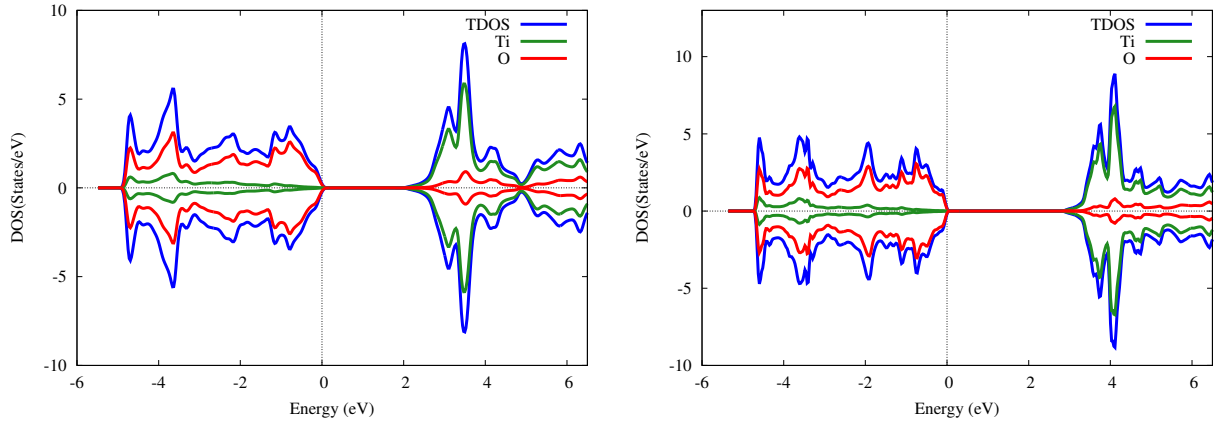

Figure 4.7: DOS of TiO_2 anatase with PBE (left) and mBJ (right) potential.

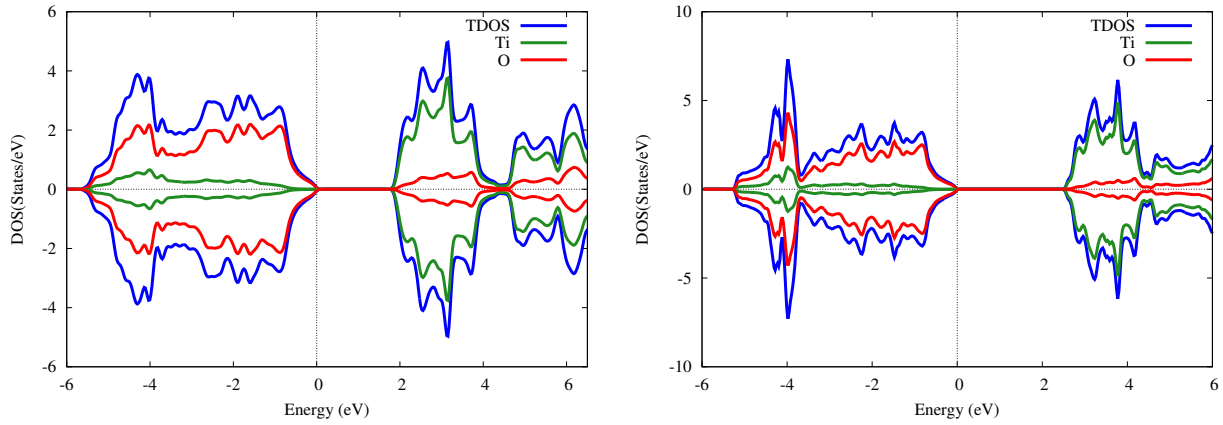

Figure 4.8: Estimated DOS of rutile TiO_2. Left for PBE and right for mBJ potential.

In the case of rutile, the valance band ranges from 5.5 to 0 eV for PBE and 5.3 to 0 eV for mBJ approximation. Band-gap found is 1.822 eV for PBE and 2.561 eV for mBJ approximation. There is a little difference between them. There are some differences in oxygen contribution between the rutile and the anatase which can be attributed to the different distortions of the O atom. The concentration of the oxygen atom is rich in valence band than conduction band in both rutile and anatase structure.

4.6 Optical properties

We also evaluate the optical absorption spectra for the TiO_2 rutile and anatase separately with either PBE and mBJ potential to simulate the optical properties of TiO_2. It absorbs mainly UV light and a very weak absorption in the visible-light region. Figure 4.9 represents the absorption coefficient versus energy curve of anatase and rutile structure for PBE and mBJ potential. We know the visible light ranges from 1.8 eV to 3.1 eV. From the figure,

we can see that there is a small energy absorption coefficient in the visible light region. Absorptivity increases in the UV region and we got a sharp peak at approximately 7 eV in anatase and approximately at 8 eV in rutile. So, both rutile and anatase mainly absorb UV light. Optical absorption provides essential information on the electronic structures of semiconductors.

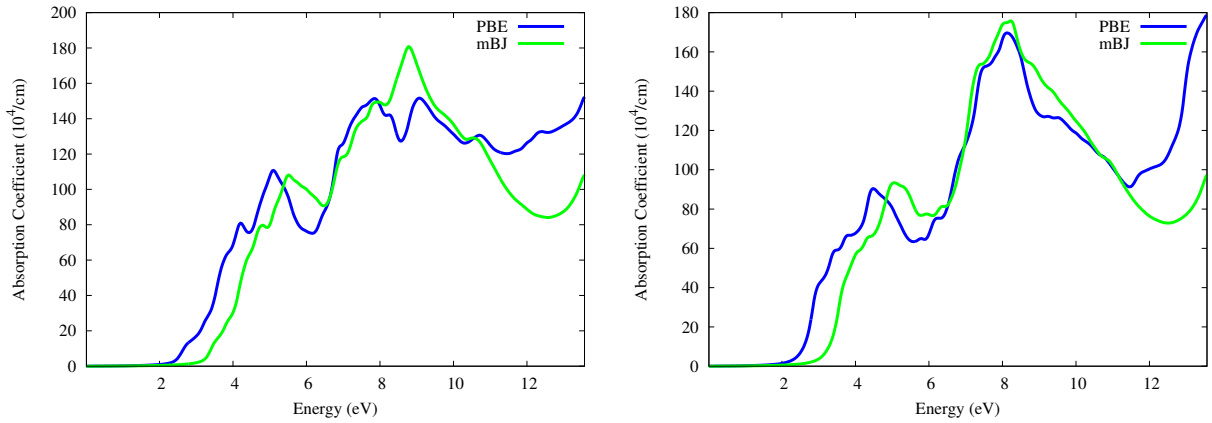

Figure 4.9: Optical absorptivity for anatese and rutile phase. Left for anatase and right for rutile.

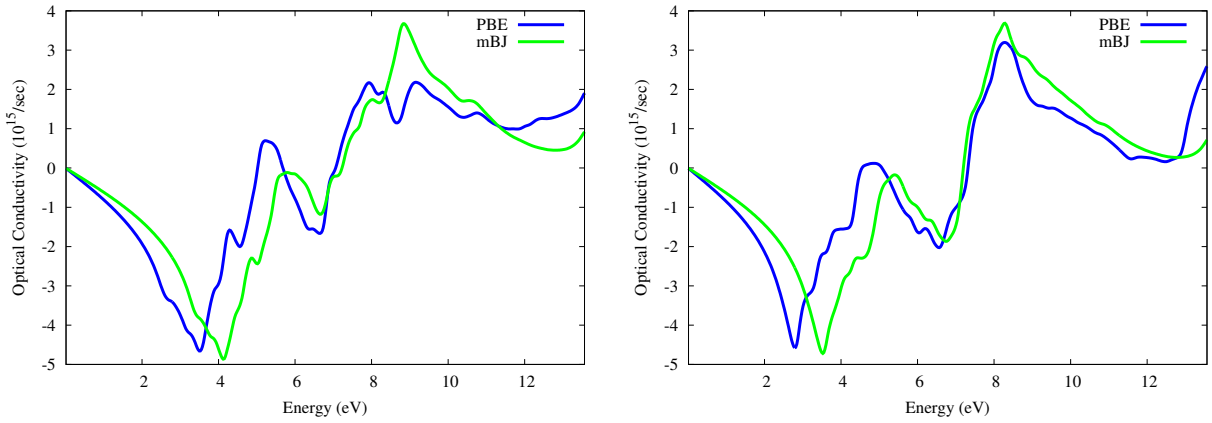

Figure 4.10: Optical conductivity for anatase (left) and rutile (right) phase.

Figure 4.10 represents the optical conductivity at different energies of anatase and rutile structure respectively. The optical conductivity is the extension of electrical transport to high (optical) frequencies. As electronic conduction is a matter of putting electrons in the conduction band, one other way to achieve this goal is to give an electron bound to the atoms enough energy to break the bond and set it free to move.

This can easily be performed by shining the material with light which photons do have energy allowing the breaking of the bonds. In a solid-state language, photons can promote electrons from the valence to the conduction band leaving a hole in the valence band. The freed electron and hole can then contribute to the electrical conduction of the material. This is called optical conductivity. Electron energy loss spectroscopy is the use of the energy distribution of electrons that pass through a thin sample to analyze the content of the sample and create images with unique contrast effects. When a photon strikes the atoms of TiO_2 it looses some energies to excite the electrons of TiO_2.

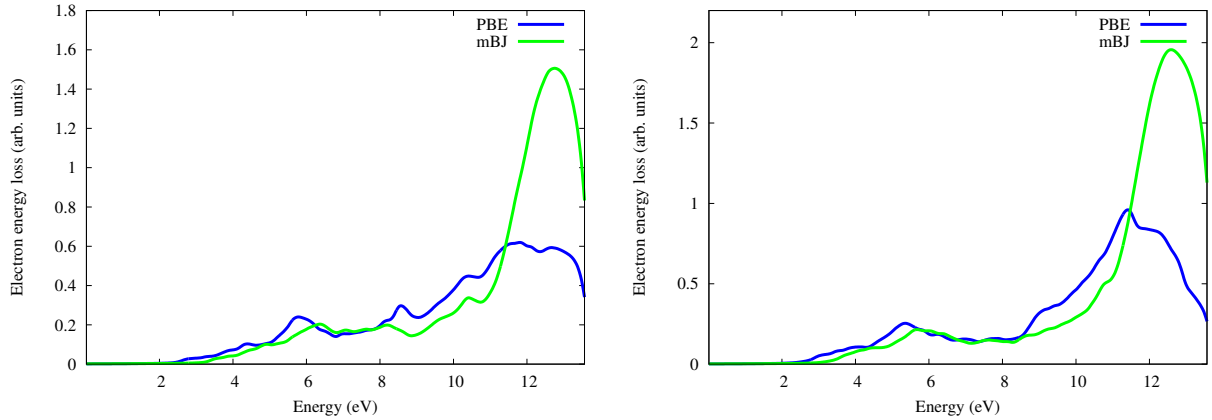

Figure 4.11: Electron energy loss for anatase and rutile structure. Left for anatase and right for rutile.

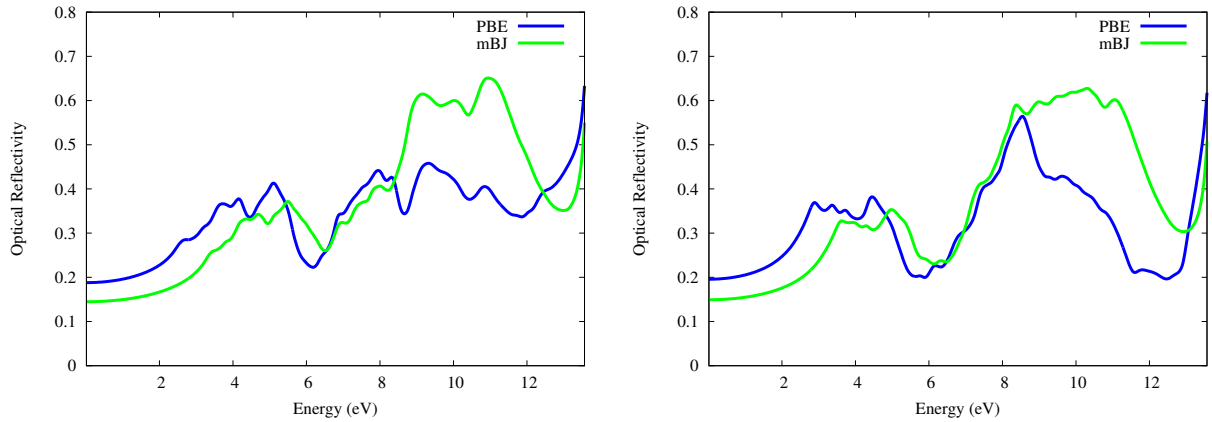

Figure 4.12: Optical reflectivity for anatase structure with PBE (left) and mBJ (right) potential.

Figure 4.11 represents the electron energy loss versus system energy for anatase and rutile structure for PBE and mBJ potential respectively. Almost 90% photon energy is needed to be absorbed by the electron for going to the next stable state. We know that reflection is the change in direction of a wavefront at an interface between two different media with different

refractive indexes. So that the wavefront returns into the medium from which it originated. When light interacts with the TiO_2 sample some photon gets reflected by the at the atomic surface of TiO_2. Reflectivity increases with the increment of energy as shown in the figure. Figure 4.12 is representing the optical reflectivity of anatase and rutile structure respectively.

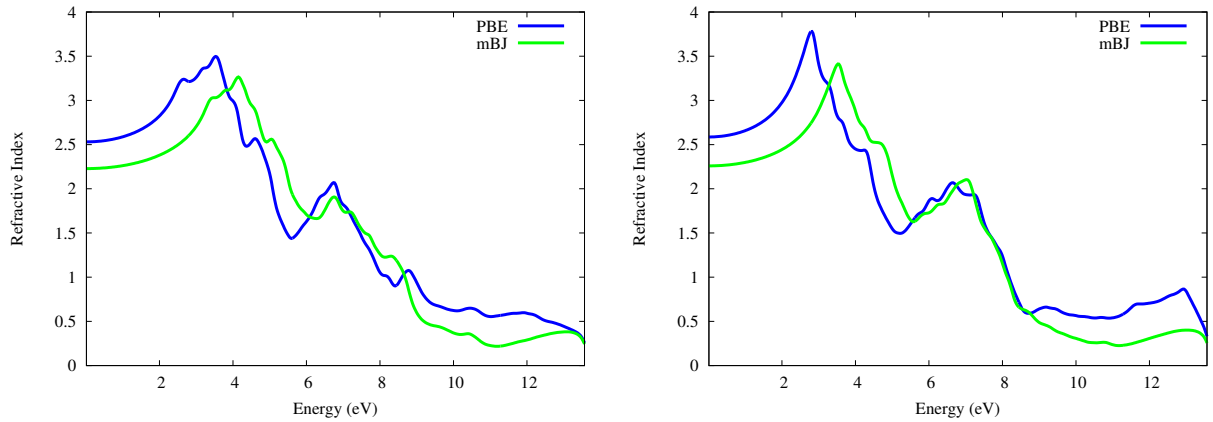

Figure 4.13: Refractive index for anatase and rutile structure. Left for anatase and right for rutile phase.

Both structure with PBE and mBJ potential gives almost the same result. The reflectivity is maximum at 10.5 to 11 eV. About refraction, we know that the refractive index means how fast light travels through the material. The real part of refractive index versus the incident photon energy for parallel polarization of electric field of an electromagnetic wave is depicted in figure 4.13. It should be noted that the refractive index is directly proportional to magnetic moment (μ) of the system, with relation N = $\sqrt{\mu\epsilon}$, that shows the dependency of refractive index to magnetic properties of them. So, the engineering of the refractive index is possible by tuning the magnetic moment. Figure 4.13 is representing the refractive index of anatase and rutile TiO_2 structure for PBE and mBJ potential respectively. For both structures, the value of the refractive index is maximum at approximately 3 eV for both potentials. From the figure, we can see that the traveling speed of light through the anatase and rutile structure increases to 3 eV but after that speed of light decreases as the energy increases with time. This means, in both anatase and rutile structures optical absorptivity and conductivity increase when it is subjected to UV light, and reflectivity and refractivity decrease in the UV region.

Chapter 5

Electronic and Optical properties of $Ti_{0.75}Nb_{0.25}O_2$

The structural and electronic properties of Nb-doped rutile TiO_2 with doping configurations were investigated by first-principles calculations based on the density functional theory [46]. The presence of Nb within the crystalline structure increased the photo-activity of powders as compared to non-modified TiO_2 powders, while the Nb deposition at the powder's surface decreased the photo-activity for all the investigated compositions. In the over a stoichiometric range of the oxide, the data, when applied to undoped rutile, allow some conclusions about the atomic or electronic transport properties, both within the high and coldness regimes. [47] The electrochemical properties of Nb-doped TiO_2 were investigated for the first time as Na-ion battery anodes. The introduction of oxygen vacancies significantly enhanced the reversible capacity of the electrode due to the improved conductivity. In pursuit of upper photo-activity, Nb-doped TiO_2 powders were evaluated within the reduction of CO_2. The replacement of Ti by Nb in the crystalline structure of TiO_2 promoted methanol formation.

5.1 Crystallographic structure

If we dope 25% Nb within pure TiO_2, the electronic structure of $Ti_{0.75}Nb_{0.25}O_2$ we found is given in figure 5.1. $Ti_{0.75}Nb_{0.25}O_2$ crystallizes at space group P2/m (No. 10), with lattice constants a = 4.582 $\AA$ b= 4.582 $\AA$ and c = 2.954 $\AA$ with the atomic position Ti_1 (0.25, 0.5, 0.5), Ti_2 (0, 0, 0), O_1 (0.35, 0.30, 0), O_2 (0.15, 0.70, 0), O_3 (0.40, 0.80, 0.50), O_4 (0.10, 0.20, 0.50) and Nb (0.50, 0, 0).

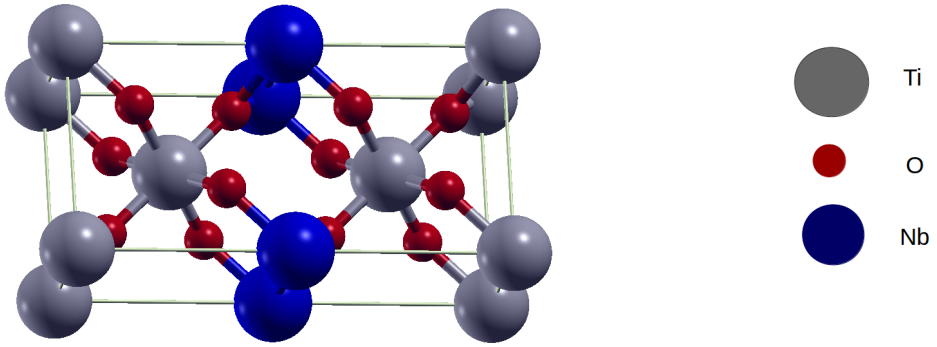

Figure 5.1: Crystallographic structure of $Ti_{0.75}Nb_{0.25}O_2$.

5.2 Volume Optimization

We perform the volume optimization calculation. The energy vs volume curve we have found from volume optimization is given in figure 5.2.

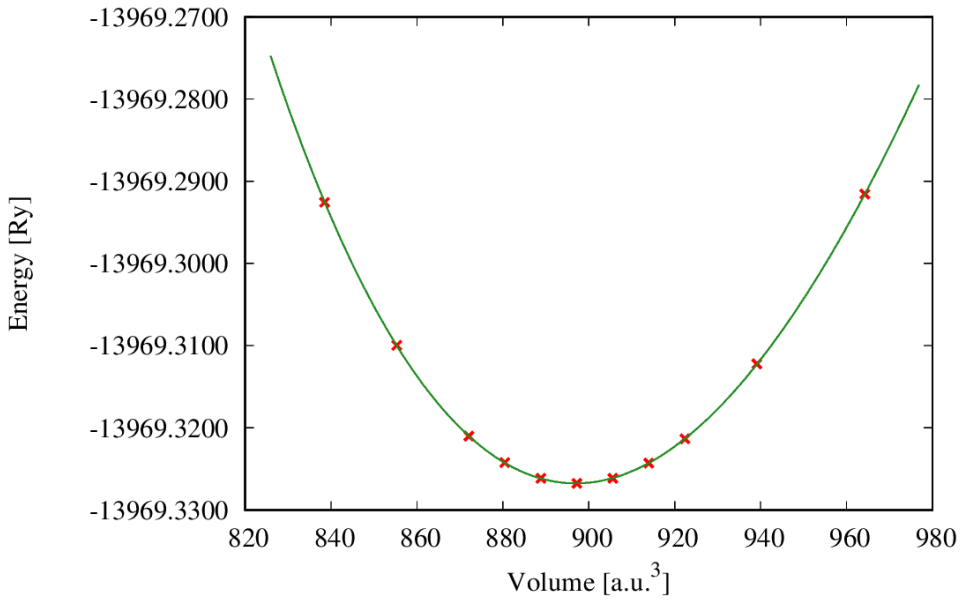

Figure 5.2: Energy vs Volume curve from Volume optimization. Lowest energy found for 6% increment from the initial structure.

We have specified the structure changes in -3, 0, 3, 6, 9, 12, 15, 18, 21 % and we have found the lowest energy structure for 6% increment from the initial value. The value of ground state energy is -13969.326745 Ry and this is the most stable structure for $Ti_{0.75}Nb_{0.25}O_2$.

5.3 Self Consistent Field (SCF)

We perform the volume optimization calculation with 1000 k-points in the first Brillouin zone. The RMT values we use is given in table 5.1. Used R_{kmax} was 7. For the SCF calculation the energy convergence value was 0.00001 Ry and the charge convergence value was 0.0001 e.

Table 5.1: RMT values used in the calculation.

Atom	RMT
Ti	1.90
O	1.70
Nb	1.90

Table 5.2: Estimated total energy (Ry) and Fermi energy for both spin and non-spin calculation with PBE and mBJ potential.

Structure	Potential	Total energy (Ry)	Fermi energy (Tetrah. M)
$Ti_{0.75}Nb_{0.25}O_2$ (non-spin)	PBE	-13969.29261854	0.6363838258
	mBJ	-13941.58720477	0.7206829829
$Ti_{0.75}Nb_{0.25}O_2$ (spin)	PBE	-13969.32606640	0.5743798328
	mBJ	-13941.57228274	0.6480336767

The total energy and Fermi energy we have found from the calculation is in table 5.2. The total magnetic moment obtained from the spin polarization of $Ti_{0.75}Nb_{0.25}O_2$ with PBE and mBJ approximation is given in table 5.3.

Table 5.3: Magnetic moments from the calculations.

Subject	Approximation	Total magnetic moment
$Ti_{0.75}Nb_{0.25}O_2$	PBE	0.55960
	mBJ	-0.08000

5.4 Energy convergence analization

Figure 5.3 and 5.4 shows how much iteration is needed to converse the enegy for the calculation. $Ti_{0.75}Nb_{0.25}O_2$ needs approximately 3 times more iteration to converse the energy.

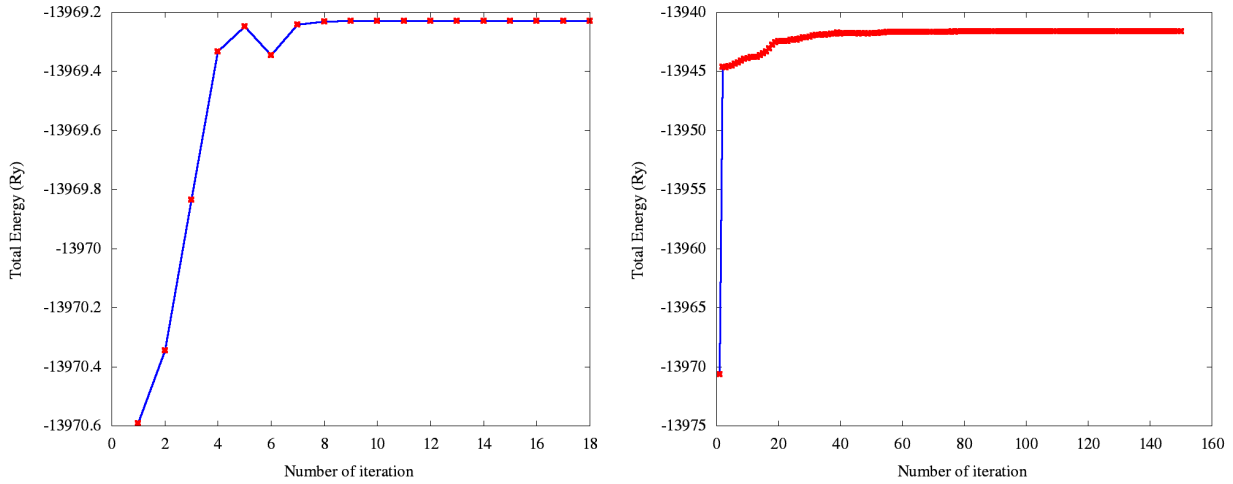

Figure 5.3: Energy convergence curve for $Ti_{0.75}Nb_{0.25}O_2$. Left for PBE and right for mBJ approximation

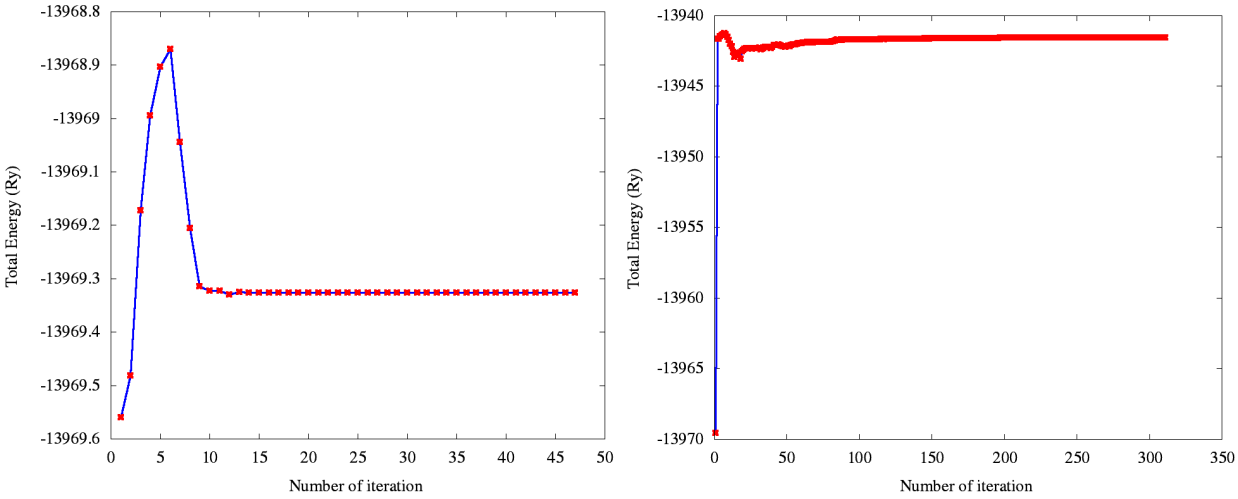

Figure 5.4: Energy convergence curve for $Ti_{0.75}Nb_{0.25}O_2$ spin polarization. Left for PBE and right for mBJ approximation

5.5 Bandstructure

Figure 5.5 and 5.6 is representing the band structure of rutile $Ti_{0.75}Nb_{0.25}O_2$ between -6 to 6 eV for PBE and mBJ potential respectively. The Valance band maximum (VBM) and conduction band minimum (CBM) is both on Γ point. We can see from the figure that conduction band is closer to the Fermi lavel than valence band and the conduction band is overlapping the Fermi lavel. For spin up and spin down the bandstructure is almost the same. Because of dopant atom (25% Nb) the samples conductivity increases.

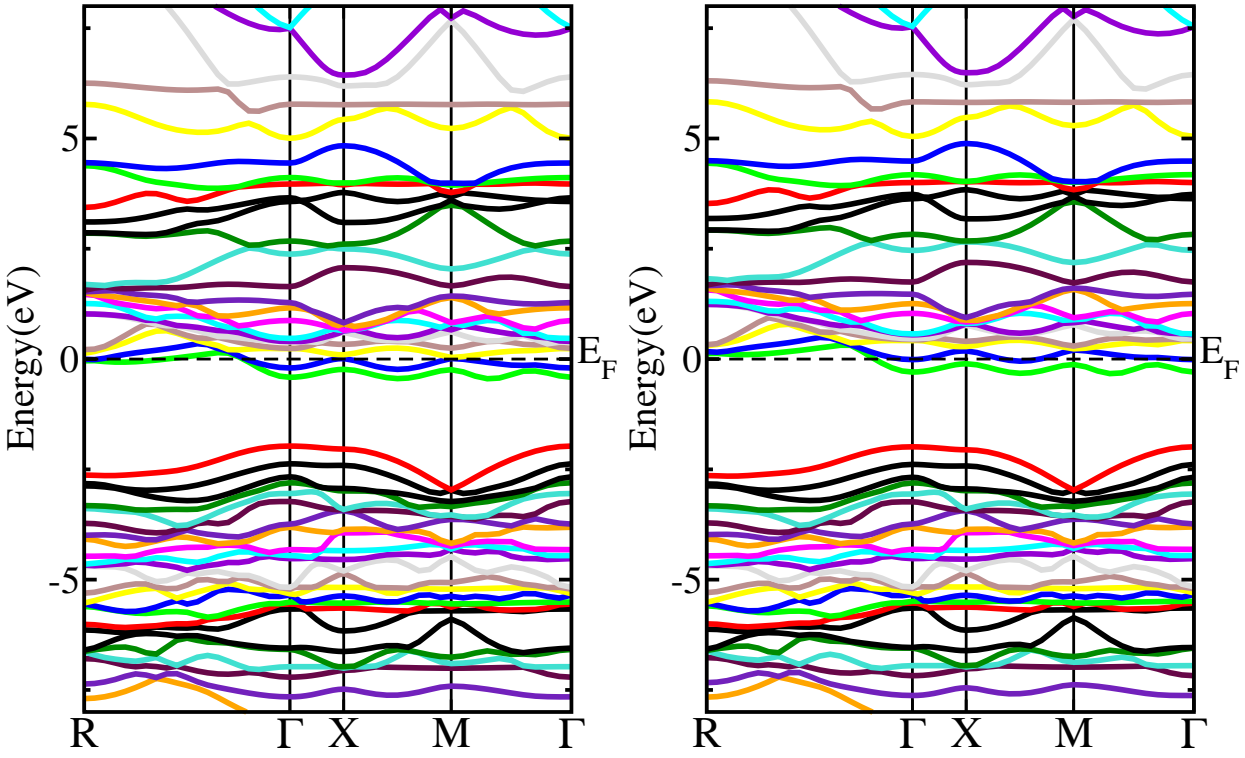

Figure 5.5: Bandstructure of $Ti_{0.75}Nb_{0.25}O_2$(rutile) for PBE potential. Left for spin up and right for spin down.

For both spin up and down with PBE and mBJ potential, conduction band is on the fermi level. so there is no direct band gap. As we know in case of metal, no direct band gap can be found. So we can state that, $Ti_{0.75}Nb_{0.25}O_2$ is showing the metallic behavior.

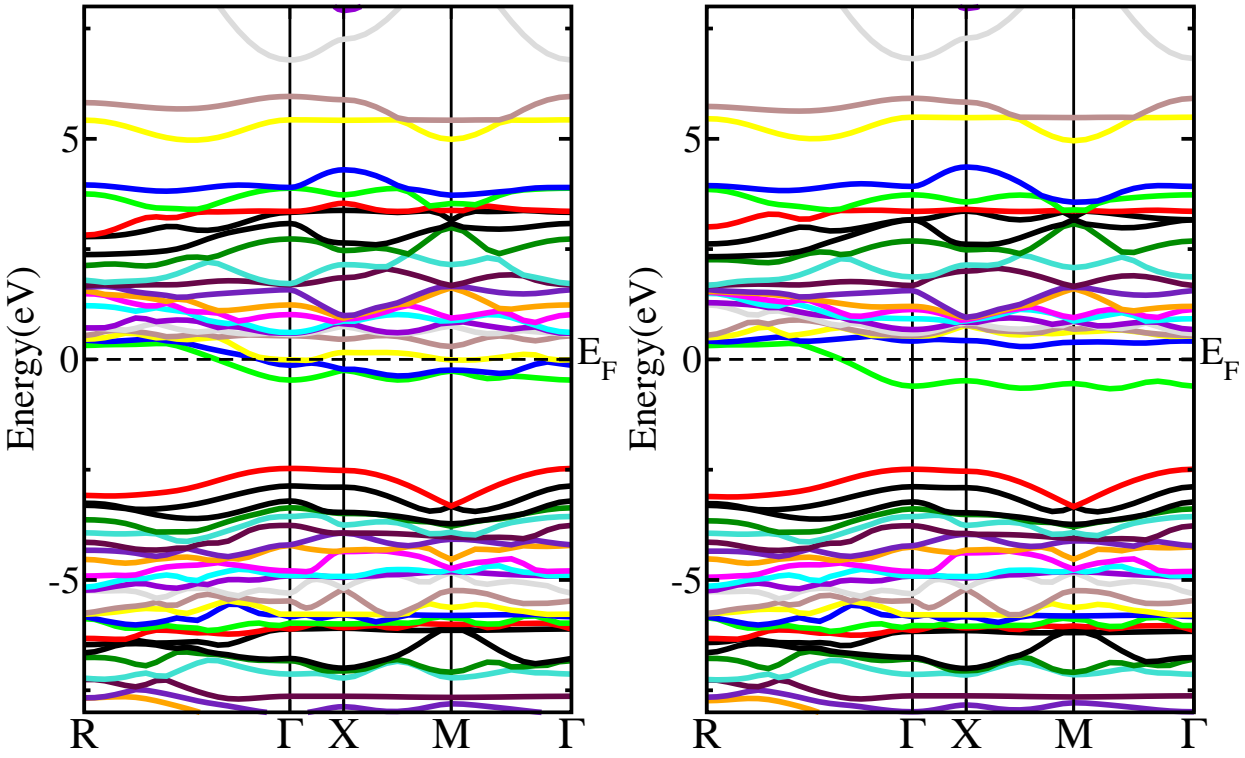

Figure 5.6: Bandstructure of $Ti_{0.75}Nb_{0.25}O_2$(rutile) for mBJ potential. Left for spin up and right for spin down.

5.6 Density of State

The added figure shows the Total density of the states(TDOS) and Partial contributions of every atoms (PDOS) that constitutes the body. From figure we can also see the energy gap between valence band and the conduction band. Conduction band is overlapping the Fermi level. So, metalic behavior is clear for $Ti_{0.75}Nb_{0.25}O_2$. The contribution of Oxygen atom is greater in valance band than conduction band but for Ti and Nb, they are rich in conduction band.

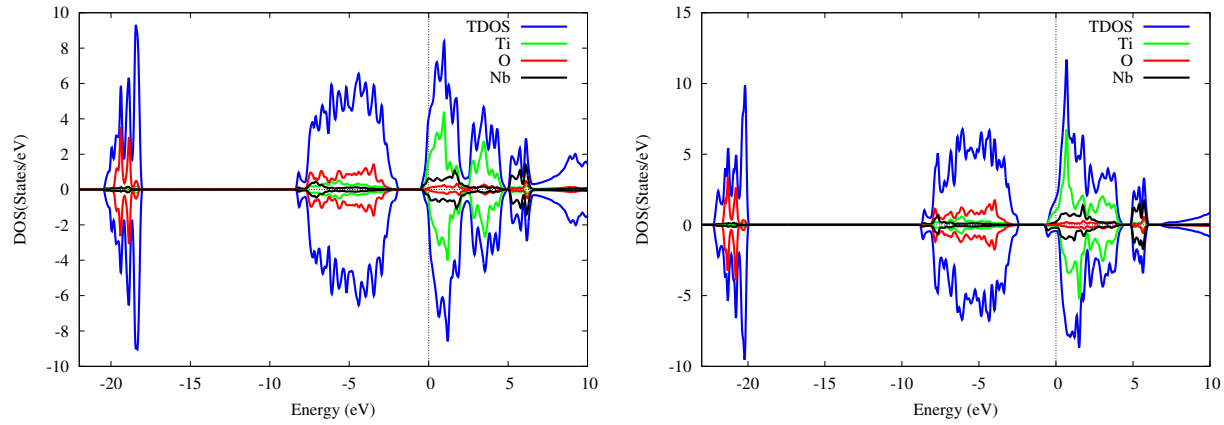

Figure 5.7: DOS of $Ti_{0.75}Nb_{0.25}O_2$ with PBE(left) and mBJ(right) potential.

5.7 Optical properties

During introducing dopant Nb on rutile TiO_2, the absorption edges extends beyond the UV light region. The optical properties in the wavelength ranges less than 400 nm are controlled by the electronic transition between O 2p states and Ti 3d states. Therefore the spectra are nearly identical in this wavelength range. The optical absorption spectra for parallel polarization of electric field of electromagnetic wave for $Ti_{0.75}Nb_{0.25}O_2$ with PBE and mBJ approximation is given below in figure 5.8.

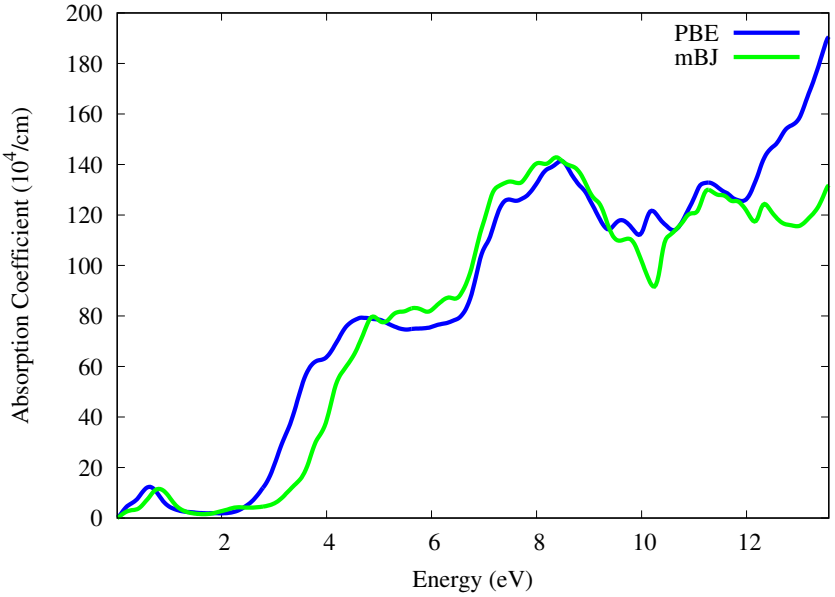

Figure 5.8: Optical absorption for $Ti_{0.75}Nb_{0.25}O_2$. Absorptivity increases beyond the visible region.

We can see from the figure that, the absorption coefficient for $Ti_{0.75}Nb_{0.25}O_2$ has a maximum value at approximately 7 eV both for PBE and mBJ potential. There is a small difference (0.1 eV) between PBE and mBJ potential. Absorptivity increases with the energy increases in the UV region. In visible region (1.8 eV to 3.1 eV) absorbtivity is negligible. Absorptivity in z-direction has a greater response than x-direction.

Figure 5.9 shows the optical conductivity for $Ti_{0.75}Nb_{0.25}O_2$. Beyond the visible region, conductivity increases and it is maximum at approximately 7 eV for both potentials. As electronic conduction is a matter of putting electrons in the conduction band, one other way to achieve this goal is to give an electron bound to the atoms enough energy to break the bond and set it free to move. Due to the inelastic scattering, an amount of energy is lost by the electrons during collision which is known as electron energy loss.

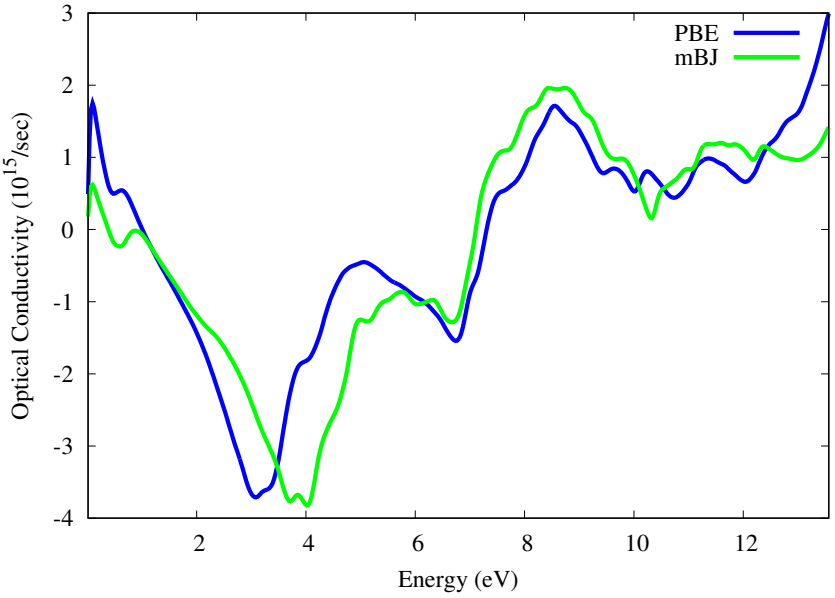

Figure 5.9: Estimated optical conductivity of $Ti_{0.75}Nb_{0.25}O_2$.

Figure 5.10 shows the electron energy loss versus Energy (eV) curve from which we can see that loss increases as the energy increases. In visible region, absorption is small so number of collisions are also small. Thats why electron energy lose is also negligible. As absorptivity starts to increase beyond the visible region, collision increases due to which loss also increases with increase energy.

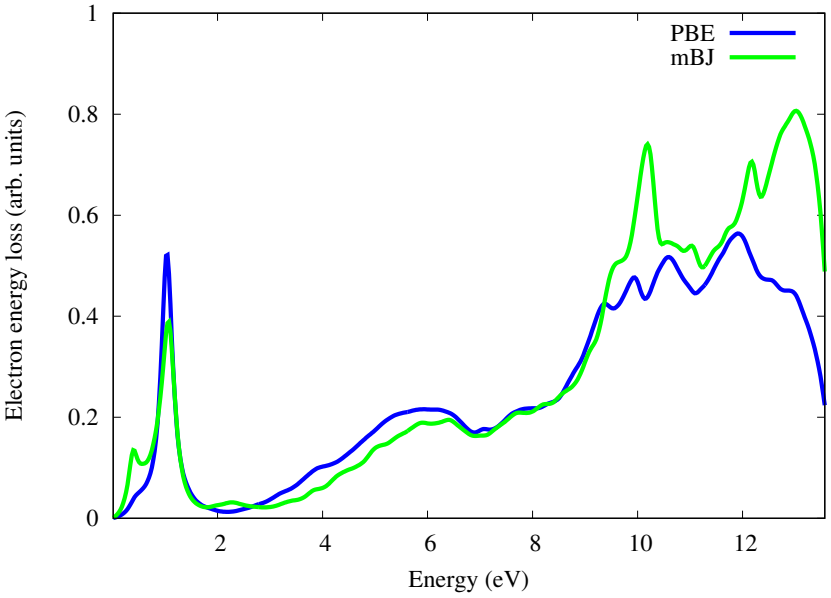

Figure 5.10: Optical electron energy loss of $Ti_{0.75}Nb_{0.25}O_2$.

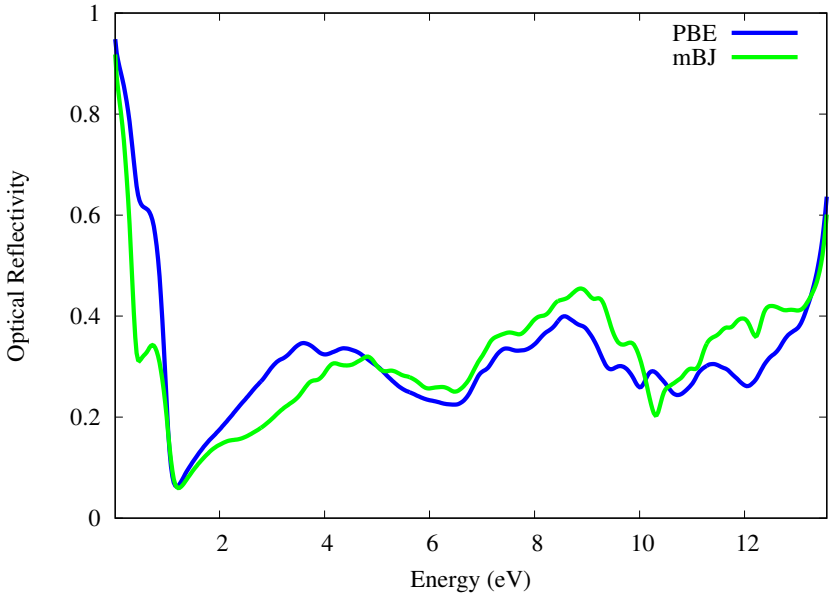

Figure 5.11: Optical reflectivity of $Ti_{0.75}Nb_{0.25}O_2$. Reflectivity decreases after visible region.

Figure 5.11 shows the optical reflection of $Ti_{0.75}Nb_{0.25}O_2$. As the reflection is inverse of the optical absorption, reflectivity in rich in visible region than UV. Figure 5.12 shows the refraction of light from $Ti_{0.75}Nb_{0.25}O_2$ surface. Refractive index decreases beyond the visible region and we get the maximum refraction in visible region. Clearly, the rutile TiO_2 is less visible-light responsive upon 25% Nb doping and the absorption strength in the visible spectrum and even in the infrared range is improved when the Nb atoms replace Ti atoms.

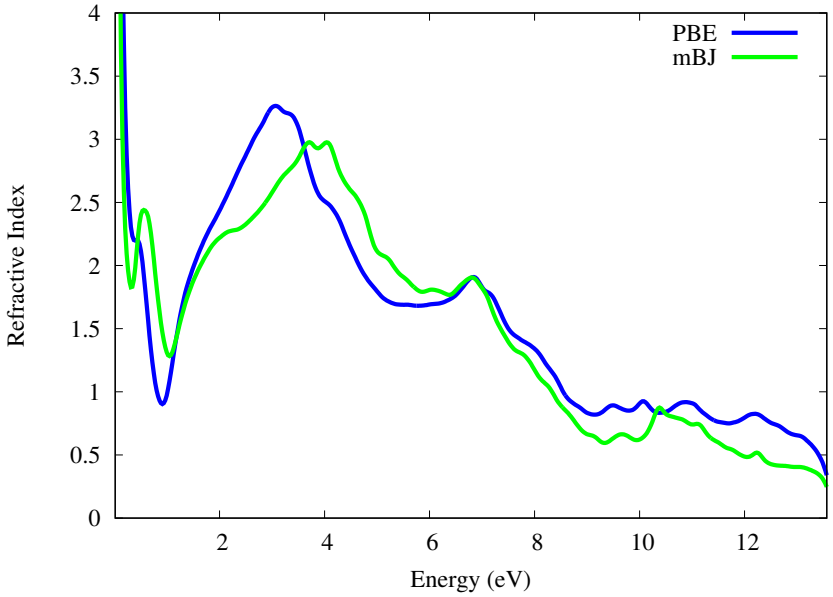

Figure 5.12: Optical refractivity of $Ti_{0.75}Nb_{0.25}O_2$.

Chapter 6

Discussion and Conclusion

In this work, we have investigated the electronic and optical properties of TiO_2 (rutile and anatase) and also for 25% Nb doped TiO_2 ($Ti_{0.75}Nb_{0.25}O_2$). Figure 6.1 is showing the band-structure of pure rutile TiO_2 and $Ti_{0.75}Nb_{0.25}O_2$.

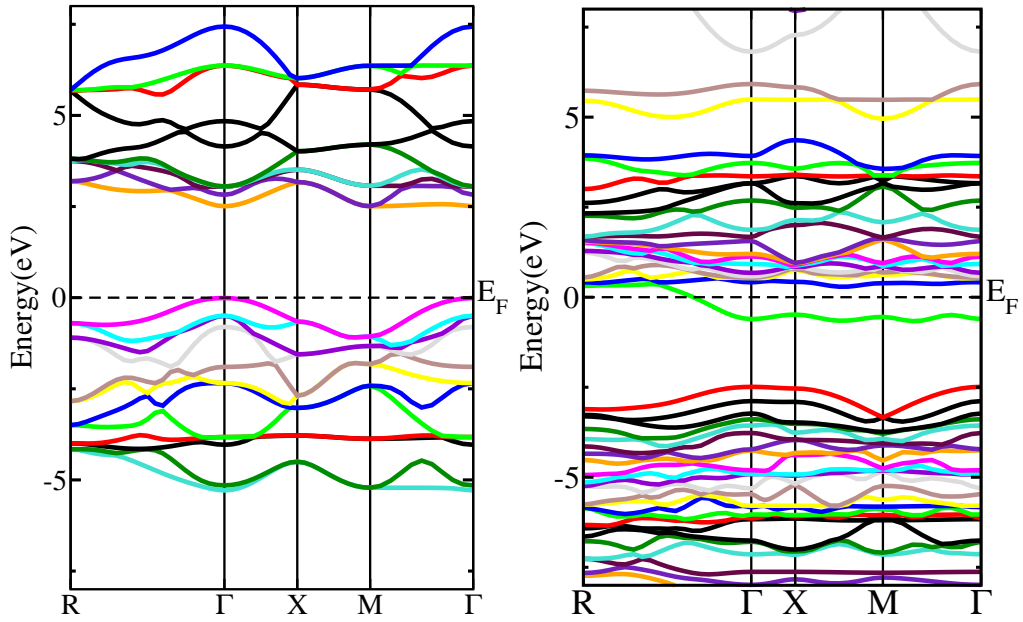

Figure 6.1: Comparison between bandstructure of pure(left) and doped rutile(right). Because of doped Nb, compound turns to a metal ($Ti_{0.75}Nb_{0.25}O_2$) from non metallic (TiO_2) behavior.

In case of pure rutile, It gives a direct bandgap which means pure rutile shows non-metallic behavior but in the case of $Ti_{0.75}Nb_{0.25}O_2$, it has no direct bandgap. So, non-metallic TiO_2 turns to a metal when 25% Nb is doped within it. We can observe a significant change in optical property in dopant TiO_2 in comparison with pure TiO_2. From figure 6.2 we can see

that absorptivity increased in visible region with dopping. Similarly the optical conductivity, electron energy loss increases with dopant Nb. reflectivity and refractivity decreases with dopand atom. Which conclude that $Ti_{0.75}Nb_{0.25}O_2$ can absorb more photon than TiO_2. So electronically and optically $Ti_{0.75}Nb_{0.25}O_2$ is more active than pure TiO_2.

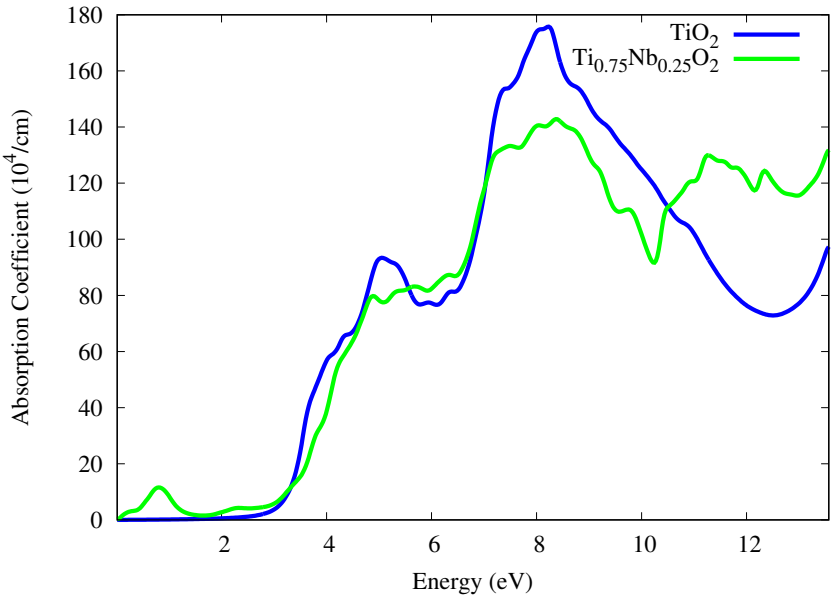

Figure 6.2: Optical absorption of pure and doped rutile TiO_2. Blue line represents pure TiO_2 and green line is representing doped TiO_2. Due to dopant Nb, absorptivity increased in visible region.

Because of increasing absorptivity, $Ti_{0.75}Nb_{0.25}O_2$ can be used instead of TiO_2 to prepare highly efficient UV-absorbing thin-film coatings for the protection of organic materials against photodegradation.

Researchers are implementing DFT to understand and predict structural, electronic, optical and magnetic properties of different materials continuously. After completing this project work, I was able to learn a lot about the electronic and optical properties of a quantum particle. In future, I wish to extend my work in this field.

List of Abbreviation

DFT	:	Density Functional Theory
RMT	:	Radius Muffin Tin
DOS	:	Density of States
GGA	:	Generalized Gradient Approximation
HK	:	Hohenberg-Kohn
KS	:	Kohn-Sham
LSDA	:	Local Spin Density Approximation
XC	:	Exchange correlation
AMF	:	Around Mean Field
FLL	:	Fully Localized Limit
RHF	:	Restricted Hartree Fock
UHF	:	Unrestricted Hartree Fock

Bibliography

[1] Zainab N. Jameel, Adawiya J. Haider, Samar Y. Taha, Shubhra Gangopadhyay, and Sangho Bok, "Evaluation of hybrid sol-gel incorporated with nanoparticles as nano paint" AIP Conference Proceedings 1758, 020001 (2016); doi: 10.1063/1.4959377

[2] P. Soni, V. V. S. Murty, K. K. Kushwaha and A. Gupta, "A Study of Nature Based Dye with Different Extracting Solvents as a Sensitizer for Dye-Sensitized Solar Cells", J. of Nanoscience Nanoengineering and Applications, vol. 8, no. 3, 2018, pp. 69-73

[3] P. Soni, V. V. S. Murty and K. K. Kushwaha, "The Effect of Ni_{2+} Ions on Energy Band Gap of TiO_2 Nanoparticles for Solar Cell Applications", Journal of Nanosci. Nanoengg. and Applications, vol. 8, no. 2, 2018, pp. 69-74.

[4] A. J. Haidera, R.H. AL-Anbarib, G.R. Kadhimb and C. T. Salame,m"Exploring potential environmental applications of TiO_2 nanoparticles", Energy Procedia, vol. 119, July 2017, pp. 332–345.

[5] A. Ayatia, A. Ahmadpour, F. F. Bamoharramc, B. Tanhaeiam, M. Mänttärid and M. Sillanpääa, "A review on catalytic applications of Au/TiO_2 nanoparticles in the removal of water pollutant", Chemosphere,vol. 107, July 2014, pp. 163-174.

[6] W. Jiang, S. Li, L. Yang and K. Du, "Experimental investigation on performance of ammonia absorption refrigeration system with TiO_2 nanofluid", Int. J. of Refrigeration, vol. 98, February 2019, pp. 80-88.

[7] S. Ali Ahmed, M. Ozkaymak, A. Sözen, T. Menlik and A. Fahed,"Improving car radiator performance by using TiO_2 -water nanofluid", Engg. Sci. and Tech., an Int. Journal, vol. 21, no. 5, October 2018, pp.996-1005.

[8] W. Wang, B. Gu, L. Liang, W. A. Hamilton and D. J. Wesolowski, "Synthesis of Rutile (α-TiO_2) Nanocrystals with Controlled Size and Shape by Low-Temperature Hydrol-

ysis: Effects of Solvent Composition", J. Phys. Chem. B, vol. 108, no. 39, September 2004, pp.14789-14792

[9] A. D. Modestov and O. Lev, "Photocatalytic oxidation of 2,4-dichlorophenoxyacetic acid with titania photocatalyst. Comparison of supported and suspended TiO_2 ", J. Photochem. Photobiol. A, vol. 112,no. 2-3, January 1998, pp. 261-270.

[10] X. Chen and S. S. Mao, "Titanium dioxide nanomaterials: synthesis, properties, modifications, and applications", Chem. Rev., vol. 107, no. 7,June 2007, pp. 2891-2959.

[11] Waghmode, M. S., Gunjal, A. B., Mulla, J. A., Patil, N. N., Nawani, N. N. (2019). Studies on the titanium dioxide nanoparticles: Biosynthesis, applications and remediation. SN Applied Sciences, 1(4), 1-9.

[12] Hohenberg P and Kohn W 1964 Phys. Rev. 136 B864

[13] Kohn W and Sham L J 1965 Phys. Rev. 140 A1133

[14] Tran F and Blaha P 2009 Phys. Rev. Lett. 102 226401

[15] Koller D, Tran F and Blaha P 2011 Phys. Rev. B 83195134

[16] Perdew J P, Burke K and Ernzerhof M 1996 Phys. Rev. Lett. 77 3865

[17] M. Born. On the quantum mechanics of collision processes (german).fuer Physik,Zeitschrift 37:863867, 1926.

[18] N. Zettili. Quantum Mechanics: Concepts and Applications . Wiley-VCH, 2009.

[19] Quantum Mechanics Concepts and Applications Second Edition Nouredine Zettili Jacksonville State University, Jacksonville, USA

[20] E. Schrödinger. An undulatory theory of the mechanics of atoms and molecules. Physical Review,28:10491070, 1926.

[21] F. Schwabl. Quantenmechanik: Eine Einführung (German) Springer, 2007.

[22] P. A. M. Dirac. A new notation for quantum mechanics of the Cambridge Philosophical Society,Mathematical Proceedings 35:416418, 1939.

[23] M. Born and R. Oppenheimer, Annalen der Physik 84, 457 (1927).

[24] L. H. Thomas, Proc. Cambridge Phil. Roy. Soc. 23, 542 (1927).

[25] E. Fermi, Rend. Accad. Naz. Lincei 6, 602 (1927).

[26] P. A. M. Dirac, Proc. Cambridge Phil. Roy. Soc. 26, 376 (1930).

[27] P. Hohenberg and W. Kohn, Phys. Rev. 136, B864 (1964).

[28] Corollary I, Richard M. Martin - Electronic structure, page 122

[29] Microscopic Mechanisms of Magnetism and Superconductivity Studied from First Principle Calculations By Zhiping Yin B. S. (Peking University) 2005, page (14-15)

[30] A. D. Becak, Phys. Rev. A 38, 3098 (1988)

[31] J. P. Perdew, J. A. Chevary, S. H. Vosko, K. A. Jackson, M. R. Pederson, and C. Fiolhais, Phys. Rev. B 46, 6671 (1992)

[32] J. P. Perdew, K. Burke, and M. Ernzerhof, Phys. Rev. Lett. 77, 3865 (1996).

[33] U. von Barth and L. Hedin, J. Phys. C: Solid State Phys. 5, 1629 (1972).

[34] V. I. Anisimov, F. Aryasetiawan and A. I. Lichtenstein, J. Phys. Condens. Matter 9, 767 (1997).

[35] Czyzyk and G. A. Sawatzky, Phys. Rev. B 49, 14211 (1994).

[36] V. I. Anisimov, I. V. Solovyev, M. A. Korotin, M. T. Czyzyk. and G. A. Sawatzky, Phys. Rev. B 48, 16929 (1993).

[37] E. R. Ylvisaker, W. E. Pickett and K. Koepernik, Phys. Rev. B 79, 035103 (2009)

[38] W. Kohn. Nobel lecture: Electronic structure of matter - wave functions and density Reviews of Modern Physics, functionals. 71:12531266, 1999.

[39] D.R. Hartree. The wave mechanics of an atom with a non-coulomb central eld. part Mathematical Proceedings of the Cambridge Philosophical i. theory and methods. Society, 24:89110, 1928.

[40] T. Flieÿbach. Mechanik: Lehrbuch zur Theoretischen Physik I (German) . Spektrum, 2009.

[41] Dambournet D, Belharouak I and Amine K 2010 Chem. Mater. 22 1173

[42] Pascual J, Camassel J and Mathieu H 1978 Phys. Rev. B18 6842

[43] Amtout A and Leonelli R 1995 Phys. Rev. B 51 6842

[44] Tang H, Lévy F, Berger H and Schmid P E 1995 Phys. Rev. B52 7771

[45] Mattsson A and Österlund L 2010 J. Phys. Chem. C 114.

[46] Yan, W., Liu, X. (2019). Niobium-doped TiO2: effect of an interstitial oxygen atom on the charge state of niobium. Inorganic chemistry, 58(5), 3090-3098.

[47] Baumard, J. F., Tani, E. (1977). Electrical conductivity and charge compensation in Nb doped TiO2 rutile. The Journal of Chemical Physics, 67(3),857-860.

[48] Usui, H., Yoshioka, S., Wasada, K., Shimizu, M., Sakaguchi, H. (2015). Nb-doped rutile TiO2: a potential anode material for Na-ion battery. ACS applied materials interfaces, 7(12), 6567-6573.

[49] Nogueira, M. V., Lustosa, G. M. M. M., Kobayakawa, Y., Kogler, W., Ruiz, M., Monteiro Filho, E. S., ... Perazolli, L. A. (2018). Nb-doped TiO2 photocatalysts used to reduction of CO2 to methanol. Advances in Materials Science and Engineering, 2018.

[50] Burdett J K, Hughbanks T, Miller G J, Richardson Jr J W and Smith J V 1987 J. Am. Chem. Soc. 109 3639

[51] Kowalczyk S P, Mefeely F R, Ley L, Gritsyna V T and Schirley A 1977 Solid State Commun. 23 161

[52] Sanjines R, Tang H, Berger H, Gozzo F, Margaritondo G and Levy F 1994 J. Appl. Phys. 75 2945

[53] Blaha P, Schwarz K, Madsen G K H, Kvasnicka D and Luitz J 2001 WIEN2k an Augmented Plane Wave + Local Orbitals Program for Calculating Crystal Properties (Austria: Karlheinz Schwarz Technische Universität Wien)